Available online at www.sciencedirect.com
ScienceDirect
Journal of volcanology and geothermal research
Journal of Volcanology and Geothermal Research 158 (2006) 401–429
www.elsevier.com/locate/jvolgeores

Eruptive dynamics of the "Citlaltépetl Pumice" at Citlaltépetl volcano, Eastern Mexico

Andrea Rossotti [a,*], Gerardo Carrasco-Núñez [a,1], Mauro Rosi [b,2], Andrea Di Muro [c,3]

[a] Centro de Geociencias Campus UNAM, Blvd. Villa del Meson s./n. Juriquilla, Qro, Mexico
[b] Dipartimento di Scienze della Terra, Via S. Maria 53, 56126 Pisa, Italy
[c] Université Pierre et Marie Curie, Laboratoire de Pétrologie Modélisation des Matériaux et Processus UMR 7160 Minéralogie et Pétrologie Case 110, Place Jussieu 4, 75252 Paris Cedex 05, France

Received 12 October 2005; received in revised form 7 July 2006; accepted 17 July 2006
Available online 12 September 2006

Abstract

Citlaltépetl (Pico de Orizaba) is Mexico's highest (5675 m a.s.l.) potentially active volcano, which is presently in a dormant state. Between 9.0 and 8.5 ky B.P., a sequence of volcanic eruptions occurred at Citlaltépetl volcano as part of the most explosive Holocene episode. This sequence is associated with the deposition of an intercalation of pumice fallout and scoria and pumice-rich pyroclastic flow deposits, named here as "Citlaltépetl Pumice" (C.P.). Detailed stratigraphic and petrographic correlation of over 100 measured sections, in conjunction with the analysis of the physical characteristics of the juvenile and lithic portions of each main layer of the sequence, provided the basis to reconstruct the eruptive episodes and to assert the eruptive dynamics of the whole sequence, which was divided into eight main eruptions separated by three brief periods of quiescence. The eruption sequence started with a phreatic phase that soon developed into a bread-crusted, bomb-bearing phase. This was followed by a sequence of vigorous Plinian explosive eruptions separated by brief periods of repose and a short dome-collapse activity. It was followed by another cycle of alternated scoria pyroclastic flows-forming and Plinian activity. This eruptive sequence shows the complexity of single eruptive events with alternated contrasting styles suggested by the compositional differences between the pyroclastic flow and fallout products.

Keywords: Pyroclastic flow deposit; Plinian; fallout deposit; Vulcanian eruptions; Citlaltépetl volcano; eruptive dynamics

1. Introduction

Citlaltépetl (also known with the name of "Pico de Orizaba") is the highest potentially active stratovolcano in North America (5675 m a.s.l.), presently in a dormant state. Its snow-capped cone (425 km^3) (Carrasco-Núñez, 2000) is located in the easternmost part of the Mexican Volcanic Belt, at the boundary between the states of Puebla and Veracruz (W 97°16′ and N 19°02′) (Fig. 1) separating the coastal side from the inner highlands with a differential relief of about 1300 m (Carrasco-Núñez, 1993).

After a detailed stratigraphic fieldwork and a new set of radiocarbon dating (Rossotti and Carrasco-Núñez, 2004), a succession of pumice fallout deposits and

* Corresponding author. Tel.: +52 1 442 2 38 11 04; fax: +52 1 55 562 34 101.
E-mail address: andrea@geociencias.unam.mx (A. Rossotti).
[1] Tel.: +52 1 442 2 38 11 04; fax: +52 1 55 562 34 101.
[2] Tel.: +39 50 22 15 7 12; fax: +39 50 22 15 800.
[3] Tel.: +33 1 44 27 51 81; fax: +33 1 44 27 39 11.

0377-0273/$ - see front matter © 2006 Elsevier B.V. All rights reserved.
doi:10.1016/j.jvolgeores.2006.07.008

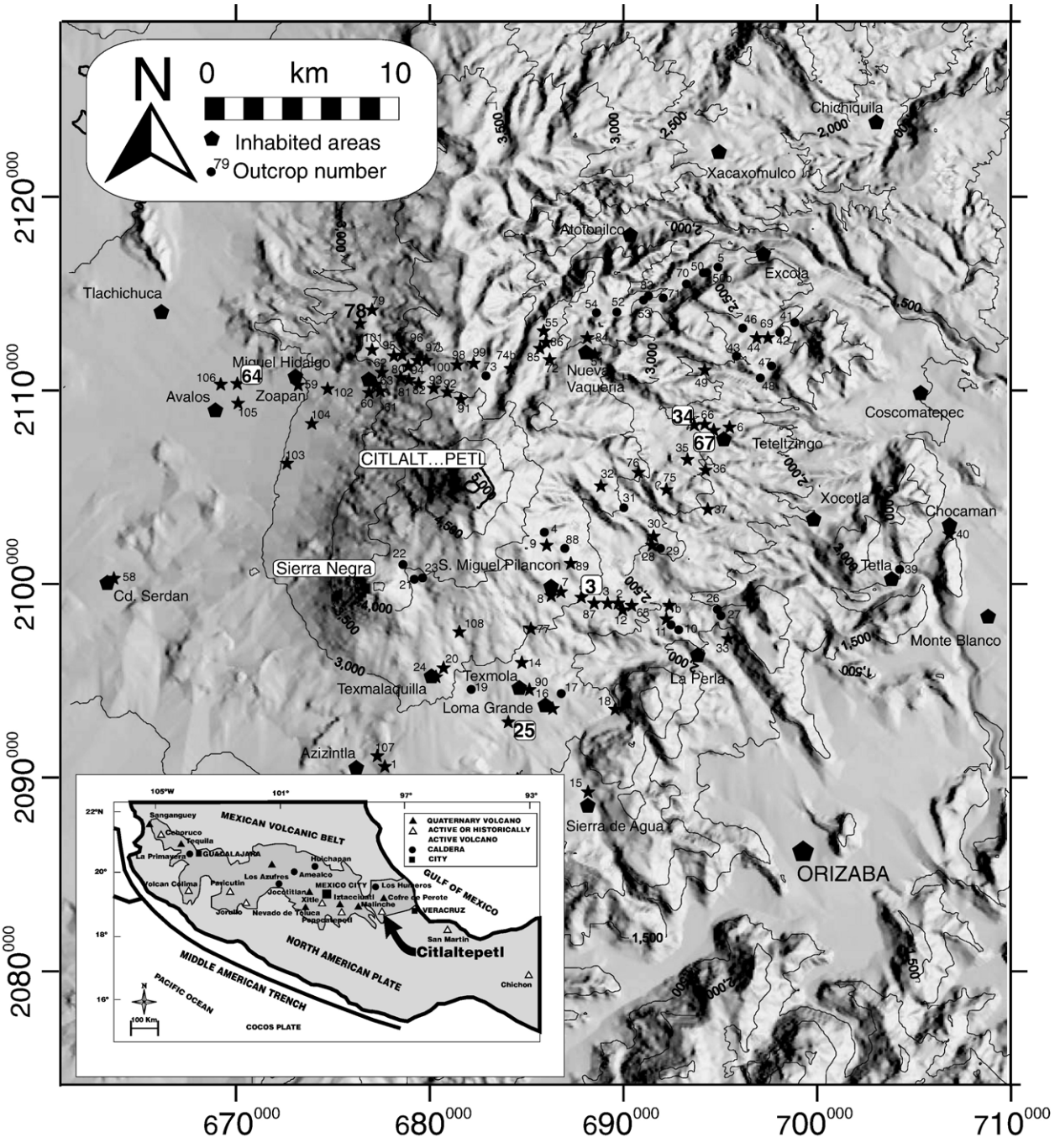

Fig. 1. Digital elevation model from INEGI, GEMA (1996), showing the location of the studied outcrops (dots) and major villages (pentagons) around the Citlaltépetl volcano. The inset map shows the location of Citlaltépetl volcano and other Quaternary volcanoes within the Mexican Volcanic Belt, Central Mexico. Larger bolt numbers represent the key sections mentioned in the text; stars are the sections where measurements for isopach and isopleth curves were performed. Interpolated results for isopachs and isopleths are shown in Figs. 7 and 9A and B, respectively.

pyrolcastic flows, named here as Citlaltépetl Pumice sequence (C.P.), were correlated with a sequence of scoria and pumice pyroclastic flows occurring about 9.0–8.5 ky B.P. and already named as Citlaltépetl Ignimbrite (Carrasco-Núñez and Rose, 1995). Here we use the terms “pumice” for a light colored (normally silicic), elongated and delicate vesicle-bearing, frothy and vitric volcanic rock formed by the sudden expansion

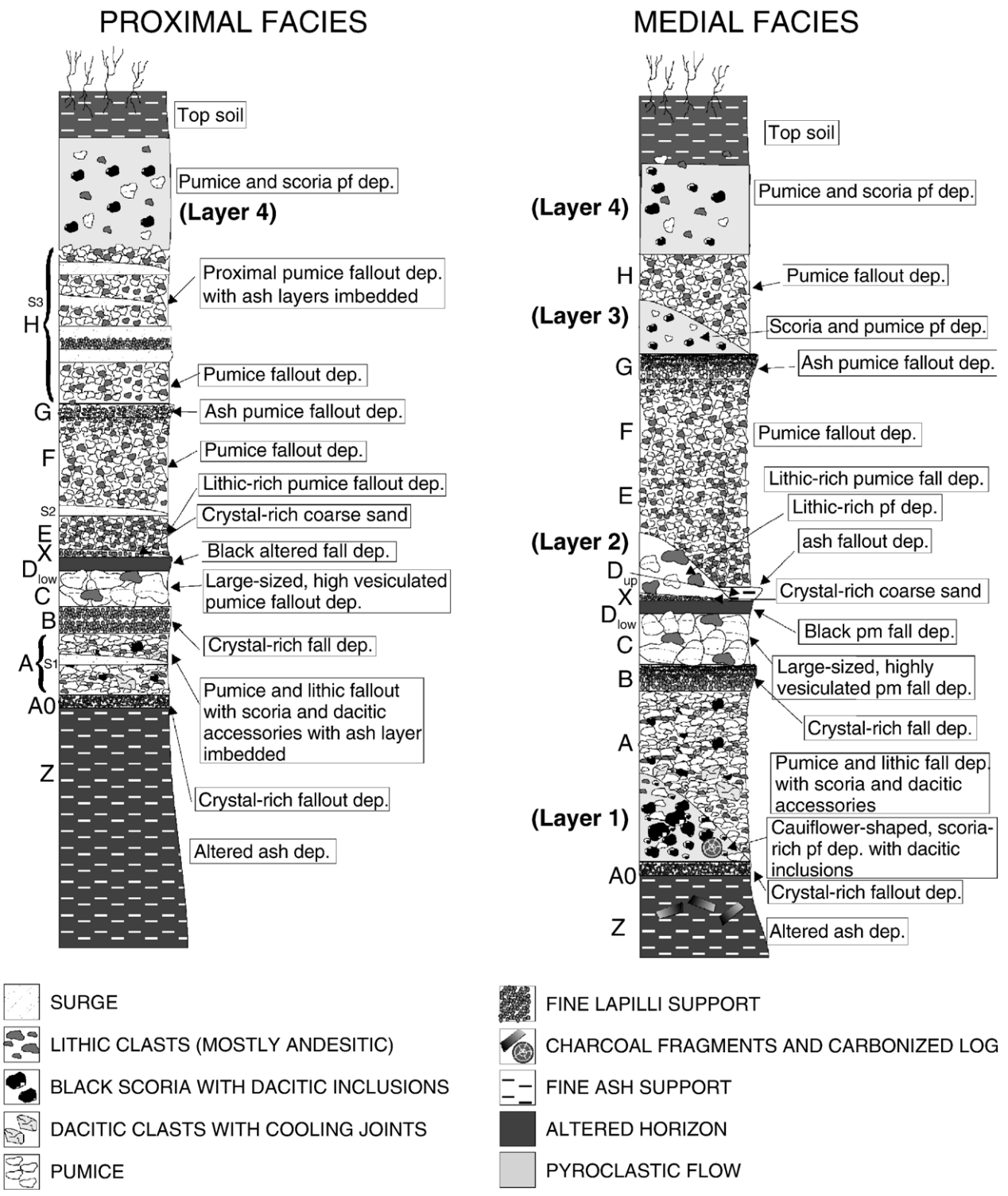

Fig. 2. Comparison of composed sections of the proximal (left) and medial to distal (right) facies of the Citlaltépetl Pumice sequence. Although sections are not at scale, relative thickness is roughly maintained among layers. Symbols size is relatively proportional to the actual grain size.

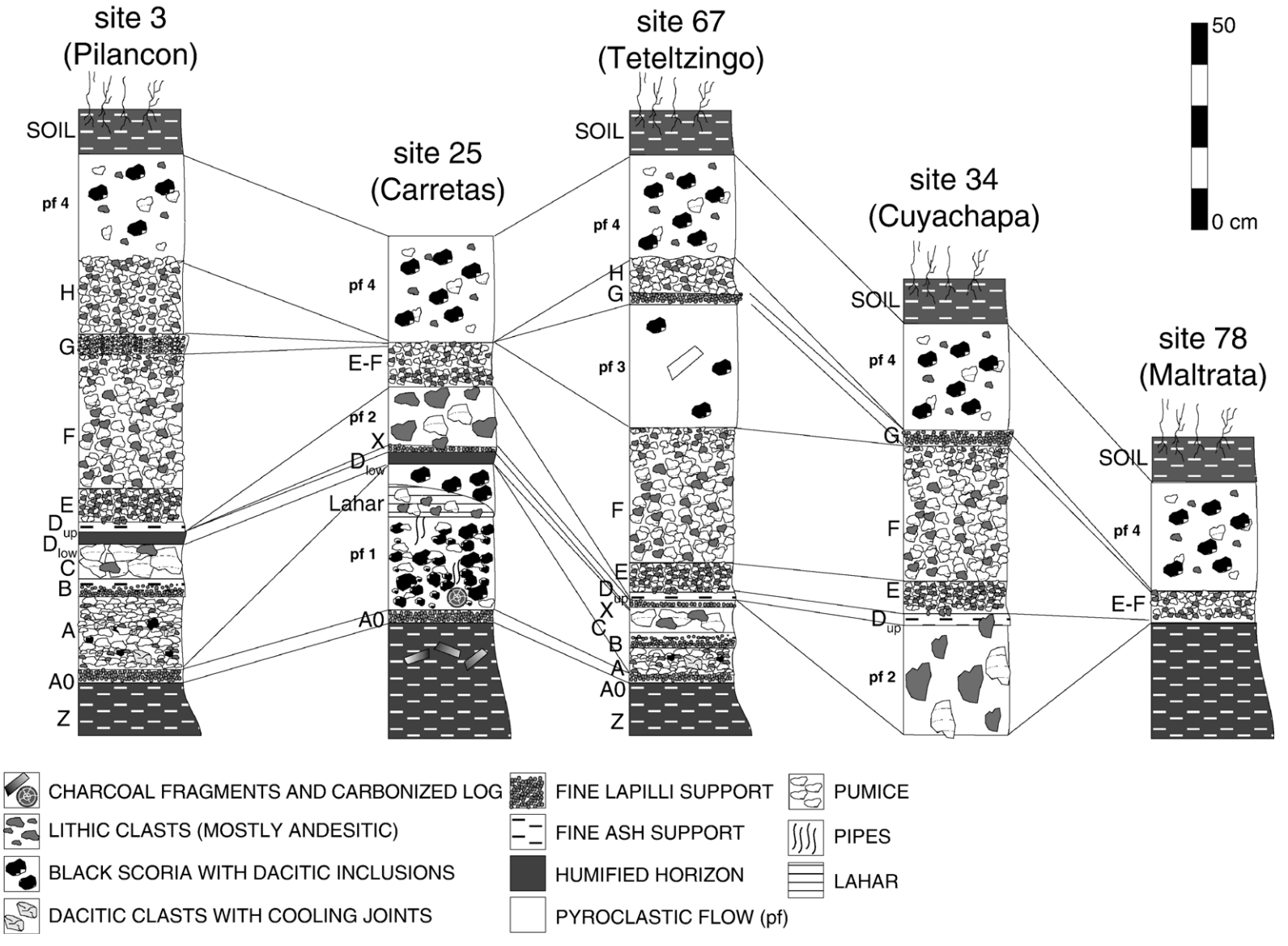

Fig. 3. Horizontal stratigraphic correlation of the outcrops showing intercalation between fallout and flow deposits. For site location, please refer to Fig. 1.

of gas in violently erupting lava, and the term "scoria" as a dark-colored (normally basaltic-to-andesitic), thick-wall, rounded vesicles-bearing pyroclast formed by the entrapment and coalescence of gas bubbles into flowing lava. In spite of the difference between the two eruptive styles, results of this new correlation indicate that the complete C.P. is therefore not only a simple tephra sequence, but a more complex pyroclastic flow and fallout deposits intercalation that clearly indicates the existence of a close alternation among two different volcanic styles. One of these, Plinian, produced intense high eruptive columns and thick pumice fallout deposits, and another (vulcanian) produced scoria-bearing pyroclastic flow deposits. We define and assume here a "vulcanian style" event as an eruption related to the formation of bread-crusted bombs and cauliflower scoria clasts associated with small pumice or scoria-rich pyroclastic flows not produced by a column collapse but more likely by a "boiling-over" activity. The purpose of this paper is to propose a model for the eruption dynamics responsible for the formation and changes in eruptive style of the C.P. Such a goal has been achieved through the analysis of the physical eruptive parameters obtained from the detailed study of the pyroclastic fallout and flow deposits and by the stratigraphic correlation of over 100 vertical outcropping profiles (Fig. 1).

2. Summary of the Citlaltépetl volcano evolution

A geological description of the Citlaltépetl volcano was first made by Robin and Cantagrel (1982). More recently, Höskuldsson and Robin (1993) studied the late Pleistocene eruptive history of the volcano, and some other studies on the most important recent deposits have been reported elsewhere (Carrasco-Núñez et al., 1997; Carrasco-Núñez, 1997, 1999). The evolution of the Citlaltépetl volcano was recently described by Carrasco-Núñez and Ban (1994) and Carrasco-Núñez (2000) who divided the Citlaltépetl volcanic history into three main "stages": (1) Formation of a large mostly effusive andesite cone (650–300 ky) that directly overlaid the Cretaceous carbonatic bedrock; the cone partially collapsed between 290 and 210 ky producing the ~20 km^3 "Jamapa" debris avalanche which traveled up to 75 km downstream ("Torrecillas Stage"). (2) Building of the dacitic "Espólon de Oro" cone at about 210 ky, which grew on the remains of the Torrecillas

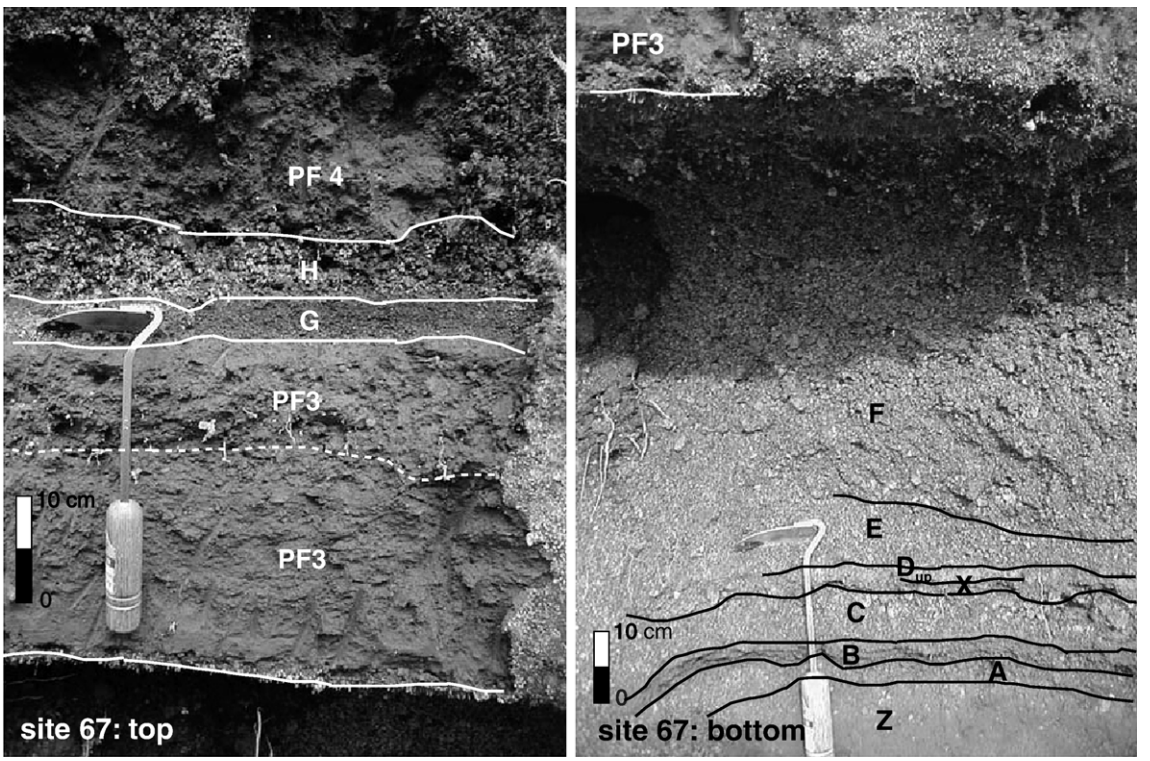

Fig. 4. Picture of the stratigraphic column outcropping at site 67 (Fig. 1), near Teteltzingo village. It shows the intercalation and respective contacts among some C.P. pumice fallout and pyroclastic flow deposits. Left picture is stratigraphically above the right one. See stratigraphic description of the respective layers for details.

Table 1
Characteristics of the C.P. pyroclastic fallout ad flow deposit layers as explained in the text

Layer	Max medial thickness	Layer color	Grading	Deposit type	Bulk density (kg/m^3)	Main distribution	Notes
Flow 4	tens of centimeters	Dark brown	Massive, ungraded	Pm-rich pf	n/a	From E to SE	Variable thick
S 3	3 cm	Gray	Laminated	pm surge	n/a	Proximal	
Fall H	20 cm	Gray -yellow	Massive to stratified	Pm fallout	630	All around the cone	Eroded at top
Flow 3	~2 m	Dark brown	Massive, ungraded	Pm-rich pf	n/a	From E to SE	Variable thick
Fall G	6 cm	Brown	Massive	Pm fallout	n/a	From NE to SE	Altered
Fall F	42 cm	Yellow	Rev. to normal grading	Pm fallout	650	All around the cone	Marker
S 2	4 cm	Gray	Stratified	pm surge	n/a	Proximal	
Fall E	10 cm	Brick red	Slight reverse grading	Pm fallout	860	All around the cone	Marker
Fall Dup	5 cm	Gray	Ungraded	Pm fallout	n/a	From N to SE	Slightly altered
Flow 2	~3 m	Dark brown	Massive, ungraded	Lth-rich pf	n/a	SE	With charcoal
Fall X	~5 cm	Gray	Ungraded	Pm fallout	n/a	SE	Discontinuous-altered
Fall D_{low}	5 cm	Black	Ungraded	Pm fallout	n/a	From N to SE	Very altered-marker
Fall C	12 cm	Yellow–pink	Ungraded	Pm fallout	680	From N to SE	Broken clasts
Fall B	5 cm	Red-brown	Ungraded	Pm fallout	n/a	From NE to SE	Altered
S 1	3 cm	Light gray	Laminated	Pm-surge	n/a	Proximal	
Fall A	50 cm	Yellow	Rev. to normal grading	Pm fallout	620	From NE to SE	–
Flow 1	~2 m	black	Massive, ungraded	sc-rich pf	n/a	SE	Bread-crusted
Fall A0	~3 cm	Gray	Slightly normal graded	lth fallout	n/a	Around the cone but NW	Broken crystal
Fall Z	>3 m	Gray-black	Massive, ungraded	Pm fallout	n/a	From E to SE	Altered and with charcoal

structure and collapsed about 16.5 ky ago (M. Sheridan, unpublished data) producing the ~2 km^3 Teteltzingo debris avalanche-induced lahar deposit (Carrasco-Núñez et al., 1993). (3) From 13 ky to the present, eruption of dacitic lavas and andesitic pyroclastic flows and fallouts which are the main constituents of the building of the present volcanic edifice. This stage includes the 8.5–9.0 ky B.P. Citlaltépetl Pumice (Rossotti and Carrasco-Núñez, 2004) that represents the most explosive phase of Citlaltépetl volcano in Holocene time.

3. Definition of the Citlaltépetl pumice

The Citlaltépetl Pumice is a volcanic sequence associated with the most explosive volcanic event in the Holocene history of Citlaltépetl volcano. The whole sequence is radiocarbon constrained between 9.0 and 8.5 ky B.P. (Rossotti and Carrasco-Núñez, 2004) and embraces a sequence of eruptive phases associated with a variation of the volcanic style from vulcanian to Plinian. As shown in Fig. 2, the proximal facies of the C.P. is dominantly composed by interbedded fallout and surge deposits (<10 km from the vent) while the medial facies is dominated by the intercalation of pyroclastic flow deposits within fallout deposits. To facilitate and simplify descriptions for the pyroclastic sequence studied here, we use the term "pumice" to define the juvenile of the entire sequence, although scoria clasts are also present in the pyroclastic flow deposits.

The whole C.P. sequence is therefore composed of (1) four centimetric to metric thick, clast supported, lapilli-sized, pumice-rich, main fallout deposits (Layers A, C, E+F, and H); (2) six thin fine-lapilli horizons (A0, B, D_{low}, X, D_{up} and G) intercalated to the main fallout deposits; (3) several thin, fine lapilli-sized, pumice-rich, pyroclastic surge-related horizons (proximal facies only); and (4) at least four main mostly scoriaceous and pumiceous pyroclastic flow deposits found mainly at the bottom of the radial narrow valleys of the cone and only recently correlated (Rossotti and Carrasco-Núñez, 2004) with the lower and upper members of the Citlaltépetl Ignimbrite (Carrasco-Núñez and Rose, 1995) and therefore included as part of the C.P. (Fig. 3).

4. Stratigraphy, petrography and chemistry of the C.P. sequence

The whole C.P. sequence, which drapes the topography around the Citlaltépetl volcano (mainly towards the eastern and southeastern flanks of the cone) up to a distance of about 25–30 km from the crater (Fig. 1), is generally sitting on a meter-thick, ash-sized pumice dark layer described below (Layer Z) and overlaid by a meter-thick soil widely cultivated. Since fallout deposits generally mantle equally the entire topography while pyroclastic flow deposits tend to concentrate into valleys, the C.P. stratigraphy largely varies in accordance with the topographic place where the outcrop was

Table 1 (*continued*)

Main components (wt.%)				Clast size	Sorting (sigma)	Vesicularity (vol.%)		Density (kg/m^3)		DRE	Modal analysis on pm clasts (vol.%)					Lower contact
pm	sc	lth	Other	Md (phi)		pm	sc	pm	sc	pm	Tot phenocr.	px	pl	aph	Glass	
20.0	10.0	30.0	40.0 Mtx	10 cm	n/a	60.94	14.60	1030	1547	2637	32.40	8.90	20.60	2.60	21.40	Erosional
68.4	0.0	31.0	0.4 L. Cry	0.36	1.76						n/a					Sharp
63.6	0.0	35.6	0.8 L. Cry	−2.71	2.06	63.98	–	897	–	2490	22.70	10.40	10.40	0.10	34.40	Sharp
30.0	5.0	10.0	55.0 Mtx	20 cm	n/a	62.71	24.80	1002	1362	2687	30.20	7.80	18.60	4.10	22.90	Erosional
70.1	0.0	29.7	0.2 L. Cry	0.54	1.72						n/a					Sharp
71.0	0.0	28.0	1.0 L. Cry	−1.55	2.06	62.76	–	975	–	2618	23.40	10.30	11.30	0.80	40.20	Faint
71.5	0.0	27.6	0.6 L. Cry	0.51	1.69						n/a					Sharp
40.0	0.0	55.7	4.3 L. Cry	−1.91	1.80	64.45	–	872	–	2453	19.20	5.60	11.60	2.00	44.50	Sharp
44.0	0.0	11.0	42.0 L. Cry	0.00	2.36						n/a					Sharp
5.0	10.0	40.0	45.0 Mtx	20 cm	n/a	61.22	11.40	1071	1605	2762	25.10	7.60	15.40	2.90	22.40	Erosional
52.4	0.0	35.7	11.9 L. Cry	0.34	1.78						n/a					Sharp
57.6	0.0	41.2	1.2 L. Cry	0.75	1.82						n/a					Sharp
64.4	0.0	33.5	2.1 L. Cry	−3.21	1.96	72.80	–	653	–	2401	33.20	5.50	26.50	0.70	15.50	Sharp
81.8	0.0	18.0	0.2 L. Cry	−1.15	2.00						n/a					Sharp
58.7	0.0	39.2	1.9 L. Cry	0.49	1.79						n/a					Sharp
63.2	0.0	33.6	3.2 L. Cry	−2.50	1.48	65.62	–	867	–	2522	13.10	6.20	6.50	0.30	36.70	Sharp
10.0	30.0	10.0	40.0 Mtx	30 cm	n/a	60.88	10.30	1036	1624	2648	30.70	10.50	16.70	2.60	35.40	Sharp
1.0	0.0	4.0	95.0 L. Cry	−1.00	1.55						n/a					Erosional
67.9	0.0	29.4	2.7 L. Cry	1.00	1.64						n/a					n/a

studied. In site 3, for instance (Fig. 1), almost the whole C.P. fallout deposit facies is outcropping, while in the *Paso Carretas* gully, at sites 25 (8 km SW of site 3), Layers A, B, C and H are missing due to the erosion caused by the emplacement of the pyroclastic flow-related Layers 1 and 4, respectively. Further field correlation analysis between sites 3, 25, 67 and 34 (Fig. 3) demonstrates that the C.P. pyroclastic flow deposits tend to concentrate only at the very bottom of the gullies (Fig. 4) and, therefore, horizontally pinch out quite abruptly in few tens of meters from their central flow axis, where the fallout deposits outcrop undisturbed. Such results suggest that the C.P. pyroclastic flows were of modest magnitude, therefore possibly associated with some non-Plinian event as described later.

Hereby we propose a detailed stratigraphic description (Table 1), supported by petrographic and chemical data (Fig. 5 and Table 2) of all the C.P. layers. Such a description generally refers to deposits outcropping mostly at a vent distance ranging from 10 to 15 km and does not include the depiction of the near-vent pyroclastic flow and surge deposits that might belong to the sequence. Main components %, grain size

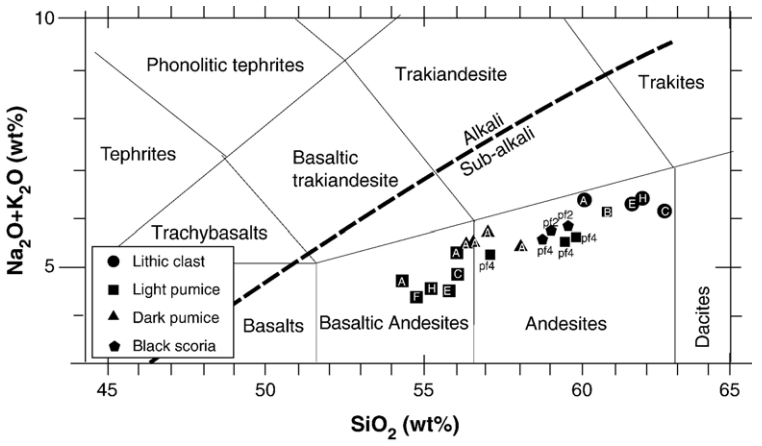

Fig. 5. Total alkali vs silica plot of pumice, scoria and lithic samples along the fallout and pyroclastic flow deposits belonging to the C.P. sequence. Letters in the samples represent the layer shown in Fig. 13. Chemical values of this plot are shown in Table 2.

Table 2
Normalized major elements values for pumice and lithic clasts of the main fallout and pyroclastic flow deposits belonging to the C.P.

%	Fallout															Pyroclastic flow					
	Dark pumice				Light pumice							Lithic clasts				Pumice			Black scoria		
	3a	30a	67a	75a	3a	3b	75a	75c	75e	75f	75h	75c	75e	75h	3a	35 (pf 4)	67 (pf 4)	67 (pf 4)	78 (pf 2)	67 (pf 3)	67 (pf 4)
SiO_2	55.5	56.0	55.1	57.7	54.7	59.7	51.8	54.1	54.4	52.5	52.8	62.7	61.4	61.6	59.6	54.71	58.19	58.78	58.98	59.81	58.31
TiO_2	1.02	0.99	1.02	0.76	1.04	0.69	1.11	0.96	0.88	0.91	0.87	0.64	0.70	0.67	0.68	0.81	0.75	0.77	0.79	0.77	0.79
Al_2O_3	17.6	18.0	17.9	17.9	18.5	18.2	19.0	19.2	18.8	19.6	19.7	17.6	17.3	17.5	17.6	19.18	17.92	16.97	16.55	16.76	17.13
Fe_2O_3	7.64	7.47	7.68	6.70	7.90	5.60	8.33	7.33	7.63	7.96	7.29	4.96	5.63	5.55	5.84	6.63	6.14	6.28	6.92	6.33	6.56
MnO	0.11	0.10	0.11	0.10	0.11	0.09	0.10	0.10	0.10	0.10	0.10	0.08	0.09	0.08	0.11	0.09	0.08	0.09	0.09	0.08	0.10
MgO	3.99	3.43	3.72	3.83	3.87	2.53	3.90	3.81	4.06	4.11	3.85	2.42	2.76	2.52	3.25	3.48	3.35	3.60	3.82	3.76	3.95
CaO	6.50	6.06	6.26	6.70	6.14	5.33	6.35	6.08	6.86	6.26	6.24	5.26	5.40	5.15	5.87	5.59	5.49	6.07	6.72	6.56	6.58
Na_2O	3.59	3.77	3.59	3.90	3.46	4.26	3.27	3.24	3.35	2.98	3.19	4.36	4.32	4.59	4.63	3.54	3.70	3.74	4.08	4.09	3.87
K_2O	1.85	1.96	1.85	1.48	1.69	1.65	1.27	1.54	1.14	1.17	1.20	1.84	1.94	1.69	1.63	1.51	1.71	1.75	1.78	1.82	1.67
P_2O_5	0.31	0.33	0.33	0.23	0.33	0.23	0.35	0.34	0.22	0.23	0.23	0.18	0.16	0.15	0.19	0.23	0.21	0.21	0.20	0.20	0.19
LOI	1.13	2.01	2.09	1.2	2.33	1.77	4.69	3.75	2.62	4.32	4.8	0.34	0.41	0.34	−0.01	4.22	2.64	1.35	0.29	0.16	1.12
Sum	99.3	100.1	99.6	100.5	100.1	100.1	100.2	100.5	100.1	100.1	100.3	100.4	100.2	99.9	99.4	100.0	100.5	99.6	100.2	100.34	100.25
Sum-loi	98.1	98.1	97.5	99.3	97.8	98.3	95.5	96.7	97.5	95.8	95.5	100.0	99.8	99.6	99.4	95.8	97.9	98.3	99.9	100.2	99.1
Total alkali	5.44	5.73	5.44	5.38	5.15	5.92	4.54	4.78	4.49	4.15	4.39	6.20	6.26	6.28	6.26	5.06	5.40	5.49	5.85	5.91	5.55
Normalized values																					
SiO_2	56.6	57.1	56.4	58.1	56.0	60.8	54.3	56.0	55.8	54.8	55.3	62.7	61.6	61.9	60.0	57.1	59.4	59.8	59.0	59.7	58.8
TiO_2	1.04	1.01	1.05	0.77	1.07	0.70	1.16	1.00	0.90	0.95	0.91	0.64	0.70	0.7	0.7	0.85	0.76	0.78	0.79	0.77	0.80
Al_2O_3	17.9	18.4	18.4	18.1	18.9	18.5	19.9	19.8	19.3	20.4	20.7	17.6	17.4	17.6	17.7	20.03	18.31	17.27	16.56	16.73	17.28
Fe_2O_3	7.79	7.62	7.87	6.75	8.08	5.70	8.71	7.58	7.83	8.31	7.64	4.96	5.64	5.57	5.88	6.92	6.27	6.39	6.93	6.32	6.62
MnO	0.11	0.11	0.11	0.10	0.11	0.09	0.10	0.10	0.10	0.10	0.11	0.08	0.09	0.08	0.11	0.09	0.08	0.09	0.09	0.08	0.10
Mg	4.07	3.50	3.81	3.86	3.96	2.57	4.08	3.94	4.17	4.29	4.03	2.42	2.77	2.54	3.27	3.63	3.42	3.67	3.83	3.75	3.99
CaO	6.62	6.18	6.42	6.75	6.28	5.42	6.65	6.29	7.04	6.53	6.54	5.26	5.41	5.17	5.90	5.83	5.61	6.18	6.73	6.55	6.63
Na_2O	3.66	3.84	3.68	3.93	3.54	4.34	3.42	3.35	3.43	3.11	3.34	4.36	4.33	4.61	4.66	3.70	3.78	3.80	4.08	4.08	3.91
K_2O	1.88	2.00	1.90	1.49	1.73	1.68	1.33	1.59	1.17	1.22	1.26	1.84	1.95	1.69	1.64	1.58	1.75	1.78	1.78	1.82	1.69
P_2O_5	0.31	0.34	0.33	0.23	0.34	0.23	0.36	0.35	0.23	0.24	0.24	0.18	0.16	0.15	0.19	0.24	0.21	0.22	0.20	0.19	0.19
Sum	100.0	100.0	100.0	100.0	100.0	100.0	100.0	100.0	100.0	100.0	100.0	100.0	100.0	100.0	100.0	100.0	100.0	100.0	100.0	100.0	100.0
Total alkali	5.54	5.84	5.57	5.42	5.27	6.02	4.75	4.95	4.61	4.33	4.60	6.20	6.27	6.31	6.30	5.28	5.52	5.59	5.86	5.90	5.60

See plot in Fig. 5.

characteristics, sorting, vesicularity, density, DRE and modal analysis values of each of the C.P. layers are summarized in Table 1.

4.1. Layer Z (altered ash layer deposited prior to the C.P. sequence)

Because of its radiocarbon age (9475±160 years B. P., Rossotti and Carrasco-Núñez, 2004), Layer Z does not properly belong to the C.P.; however, since it is always in direct contact with the C.P. base, we include its description in this work.

Layer Z is an over 3-m-thick, gray to black, massive and ungraded, ash-supported pumice-rich fallout deposit (Fig. 2 and 4 and Table 1). Its topmost part, very dark and deeply altered, shows scattered charcoal chunks used for carbon dating (Rossotti and Carrasco-Núñez, 2004). The layer is constituted mainly of pumice, lithics and a minor amount of loose crystals dispersed in the fine fraction. As for all of the layers showing an ash-sized granulometry, the vesicularity, density and modal analysis on their components were not calculated due to the too small size of the clasts. The Layer Z lower contact is unknown.

4.2. Layer A0 (phreatic crystal-rich fallout deposit)

Layer A0 is a 3-cm-thick, light-gray, slightly normally graded lithic-rich fallout deposit (Fig. 2 and Table 1). Layer A0 is always present at the base of the lowermost scoria flow deposit (Layer 1) and is more difficult to identify on topographic height sections where it appears as a discontinuous layer, underlying Layer A. Its distribution was recognized all around the cone a part than in the NW area, up to a distance of over 15 km form vent. The layer is mainly composed of broken crystals of pyroxene (65 wt.%) and plagioclase (30 wt.%) derived from fragmented lithic clasts, some sharply broken, gray, andesitic clast (3 wt.%), traces of shards (type 1 in shape, Wohletz, 1983) of transparent juvenile glass (1 wt.%) and rare fine and broken pumice (1 wt.%). Layer A0 lower contact is erosional with Layer Z. Despite the rare presence of juveniles, Layer A0 has been associated with a precursor, conduit-unplugging, phreatic eruption, due to the dominant abundance of lithic clasts.

4.3. Layer 1 (vulcanian scoriaceous pf deposit)

Layer 1 is a 2-m-thick (~20 m aside from the valley axis), black, massive and ungraded, matrix-supported scoria-rich pyroclastic flow deposit (Fig. 2 and Table 1). It was found at the bottom of the valleys running radially along the southeastern flank of the volcano. The deposit is mainly constituted of 30 wt.% of andesitic bread-crusted, cauliflower-shaped scoria bombs; 10 wt.% of rounded pumice with white dacitic inclusions in them (diagnostic), 10 wt.% of sub-angular andesitic clasts, and around 40 wt.% of fine matrix. Pumice clasts show rounded vesicles with a diameter up to 4 mm and with relatively thick inter-bubble walls. Clastic components show an average clast size up to 30 cm in diameter. In site 25 (*Paso Carretas* gully) (Figs. 1 and 3) large carbonized logs and branches embedded and well preserved at the base of the deposit were used for carbon dating (Rossotti and Carrasco-Núñez, 2004). The upper part of the deposit shows abundant sub-metric degassing pipe structures. The Layer 1 lower contact is erosional but sharp with Layer A0. The deposit tends to pinch out laterally and disappear within 50 m from the studied outcrop, so that the underlying fallout layers, usually eroded away by the overridding pyroclastic flows, are preserved in outcrop. Layer 1 has been associated with the first C.P. vulcanian phase.

4.4. Layer A (Plinian pumice fallout deposit)

Layer A is a 50-cm-thick, yellowish, reverse-to-normal graded, clast supported, pumice fallout deposit with a bulk density of 620 kg/m^3. (Figs. 2 and 4 and Table 1). It was recognized mainly at the eastern quadrants of the cone (see Layer A isopach and isopleth curves below), mainly towards the SE direction, up to a distance of about 15 km from the vent. The layer is composed of pumice, angular lithic clasts and loose crystals scattered among the fines. Layer A is mainly characterized by the presence of three different pumice types, which in order of abundance are light-yellow, black and banded pumice. Light-yellow pumice, showing a glassy matrix with thin bubble walls and elongated to fibrous vesicles, has a basaltic–andesitic composition (Fig. 5 and Table 2) and contains submillimetric plagioclase, pyroxene phenocrysts and amphiboles phenocrysts. Black pumice, showing more rounded vesicles with a diameter up to 6 mm and with relatively thick inter-bubble walls, has a composition between basaltic–andesitic and andesitic (Fig. 5 and Table 2) and contains slightly less plagioclase (5.5 vol.%), lesser pyroxene (3.5 vol.%) but relatively abundant amphibole phenocrysts (10.1 vol.%). Some dacitic white inclusions are scattered in the black clasts. Banded pumice is more scoriaceous (i.e., inter-bubble walls are thicker) with respect to light colored pumice with often bigger and more rounded vesicles in the dark

bands but with no variation in vesicularity between dark and light bands. Based mainly on grain size characteristics, Layer A was subdivided into three parts. The lower one, up to about 20 cm in thickness, is generally finer than the rest of the layer, with mean clast diameter of Md = −1.96 Φ and mean sorting of σ = 1.26. The middle part, up to 15 cm in thickness, is generally the coarsest part of the entire layer (Md = −3.02 Φ) and shows a sorting of σ = 1.55. The topmost part has 5–10 cm of thickness, with a mean clast diameter of Md = −2.52 Φ and a sorting of σ = 1.63. The Layer A lower contact with Layer A0 is sharp. Layer A has been associated with the first C.P. Plinian phase.

4.5. Layer S1 (proximal pumice-rich surge deposit)

Layer S1 is a 3-cm-thick, light-gray, clast supported, laminated pumice-rich horizon (Fig. 2 and 6 and Table 1). It was found around the cone, only at a distance closer than 10 km from the vent. It is composed of 58 wt.% of lapilli-sized, clear and relatively dense pumice, 39.2 wt.% of angular, gray andesitic clasts and 1.9 wt.% of loose crystals dispersed in the rare matrix. Such a horizon is intercalated within Layer A and its lower and upper contacts are sharp due to sudden granulometric changes. Layer S1 has been associated with an inter-Plinian surge event recorded only at proximal vent distances.

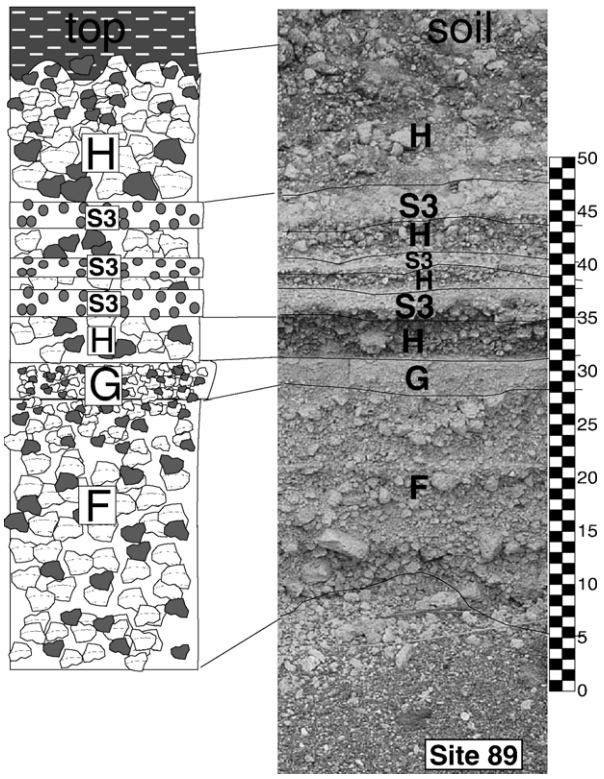

Fig. 6. Stratigraphic vertical relationship among fallout and surge deposits encountered in the proximal area of the cone. Please refer to the stratigraphic description of S layers for details.

4.6. Layer B (column collapse pumice fallout deposit)

Layer B is a 5-cm-thick, red-brown, ungraded and relatively compacted pumice-rich fallout deposit (Fig. 2 and 4 and Table 1). Its 5-cm isopach (not shown in this paper) was recognized around the cone but slightly elongated towards the eastern quadrants of the cone, up to a distance of almost 15 km from the vent. The layer, whose topmost part is slightly altered, is mainly constituted of 81.8 wt.% of andesitic pumice (Fig. 5 and Table 2), 18.0 wt.% of angular lithic clasts and just 0.2 wt.% of loose, ash-sized crystals. The Layer B lower contact is sharp with Layer A due to a strong granulometry and color contrast which suggest that the Layer B is the first resumed sustained column fallout deposit.

4.7. Layer C (Plinian pumice fallout deposit)

Layer C is a 12-cm-thick, yellow-pink, ungraded, clast supported, pumice fallout deposit (Figs. 2 and 4 and Table 1). Its distribution has been recognized from the north to the ESE side of the cone, up to a distance of 14 km from the vent (see isopach and isopleth curves below). The layer's components are mainly large jig-saw-broken, low-density, fragile pumice lapilli, basaltic–andesitic in composition (Fig. 5 and Table 2), angular lithic clasts and ash-sized loose crystals. Pumice clasts show a strong vesicularity (Table 1) with slightly elongated vesicles with a diameter up to 15 mm and with relatively thin and delicate inter-bubble walls. The Layer C lower contact with Layer B is sharp due to the strong clast size difference. Layer C has been associated with the second Plinian phase.

4.8. Layer D_{low} (humified pumice fallout deposit)

Layer D_{low} is a 5-cm-thick, black, ungraded and very altered pumice-bearing fallout deposit (Fig. 2 and Table 1). Its distribution is similar to that of Layer C. Due to its characteristic black alteration and its widespread distribution, this layer was used as a regional stratigraphic marker. It is constituted of pumice, lithic clasts and loose fine crystals. The Layer D_{low} lower contact is sharp due to the strong color contrast with the adjacent horizons. Due

to its high degree of humification, Layer D_{low} has been associated with the first time break of the C.P. sequence.

4.9. Layer X (reworked pumice fallout deposit)

Layer X is a 5-cm-thick, gray, loose, ungraded, pumice-bearing reworked deposit (Figs. 2 and 4 and Table 1). It was found mainly towards the Southeastern flank of the cone. In several places, Layer X shows a strong alteration that makes it difficult to recognize the components which are pumice, rounded and altered andesitic clasts, and loose fine crystals. Layer X is not always present in the stratigraphic columns, but can be found either overlying, in sharp contact, Layer C or D_{low}. Together with Layer D_{low}, Layer X has been associated with the first time break of the C.P. sequence.

4.10. Layer 2 (dome collapse non-vesiculated clasts-rich pf deposit)

Layer 2 is a 3-m-thick (~20 m aside from the valley axis) dark-brown massive and ungraded, matrix-supported, non-vesiculated clasts-rich pyroclastic flow deposit (Figs. 2 and 3 and Table 1). It was mainly found by the gullies running upon the SE flank of the cone, at a distance of 12.3 km from the vent (site 25 of Fig. 1: "Paso Carretas"). The deposit shows at the bottom the presence of abundant carbonized logs and branches used for carbon dating (Rossotti and Carrasco-Núñez, 2004). The main components of the layer are fine matrix, sub-angular andesitic accessory clasts (Fig. 5 and Table 2), cauliflower-shape andesitic scoria bombs (Fig. 5 and Table 2) and rounded and altered pumice showing rounded vesicles with a diameter up to 3 mm and with relatively thick inter-bubble walls. The average clast size of the deposit is around 20 cm in diameter and its lower limit with Layer X is sharp which shows partial topmost erosion. Like Layer 1, Layer 2 also tends to pinch out abruptly within a few tens of meters from the river axis, allowing the Layer X to outcrop in stratigraphic erosional contact with Layer D_{up}. Layer 2 has been associated with a dome collapse phase.

4.11. Layer D_{up} (co-ignimbrite fallout deposit)

Layer D_{up} is a 5-cm-thick, gray and ungraded and relatively compacted pumice-rich fallout deposit (Figs. 2 and 4 and Table 1). Like D_{low}, the Layer D_{up} distribution mimics the Layer C distribution, continuously covering the most part of the eastern sector of the volcano. The Layer D_{up} horizon shows similar physical characteristics of D_{low} but it is less altered. Its main components are pumice, lithic clasts and loose crystals dispersed among the fines. The Layer D_{up} lower contact with the Layer 2 deposit and with the fallout X (when both present) is sharp mainly due to the difference in granulometry, while the contact with D_{low} (when both the Layer 2 deposit and Layer X are missing) is so faint and unclear that the two layers can be considered together. Layer D_{up} has been considered as the co-ignimbrite facies deposit of Layer 2.

4.12. Layer E (Plinian pumice fallout deposit)

Layer E is a 10-cm-thick, brick-red, slightly reversed, clast supported, lithic-rich, pumice fallout deposit (Figs. 2 and 4 and Table 1). Its constant presence around the volcano, recognized up to a distance of 21 km from the vent (see isopach and isopleth curves below), mimics the Layer F distribution described below. Layer E is constituted of yellowish, basaltic–andesitic pumice (Fig. 5 and Table 2), sub-angular andesitic clasts, often oxidized or altered by a translucent thin Mn-coating, and fine loose crystals scattered in the rare matrix. Pumice clasts show sub-elongated vesicles with a diameter up to 4 mm and with relatively thin inter-bubble walls. Due to its constant radial thickness, its abundant lithic presence and its characteristic overall dark-red color, Layer E has been chosen as the main stratigraphic marker for the entire sequence. Due to the great difference in clast size, color and lithic abundance, the Layer E limit with Layer D_{up} is very sharp and noticeable. Layer E was associated with the third C.P. Plinian phase.

4.13. Layer S2 (proximal pumice-rich surge deposit)

Layer S2 is a 4-cm-thick, light-gray, clast supported, laminated pumice-rich horizon (Figs. 2 and 6 and Table 1). It was recognized around the cone, only at a distance closer than 10 km from the vent. It is composed of lapilli-sized, clear and relatively dense pumice, angular, gray andesitic clasts and loose crystals dispersed in the rare matrix. Such a horizon is intercalated between Layer E and Layer F but its lower and upper contacts are shown just by sudden granulometric contrast with the two adjacent layers. Layer S2 was associated with another inter-Plinian surge event recorded only at proximal vent distances.

4.14. Layer F (Plinian pumice fallout deposit)

Layer F is a 42-cm-thick, light-yellow, reverse-to-normal graded, clast supported, pumice fallout deposit

(Figs. 2, 4 and 6) and Table 1). The Layer F deposit outcrops around the cone and was recognized up to a distance of 37 km from the vent (see isopach and isopleth curves below). It is mainly composed of angular and light-yellow basaltic–andesitic pumice (Fig. 5 and Table 2), gray, angular, andesitic clasts and fine loose crystals. Pumice clasts show sub elongated vesicles with a diameter up to 7 mm and with relatively thin inter-bubble walls. The average clast size of the deposit is −2.05 Φ in the lower part and −1.05 Φ at the top and its average sorting is 2.16 σ at the bottom and 1.96 σ in the upper part. Although Layer F was here separately described from Layer E, we consider both layers products of a single event since the distribution is similar and the contact among them is always gradual and continuous. Together with Layer E, Layer F was associated with the third C.P. Plinian phase.

Table 3
Area (A) and thickness (T) of the C.P. main fallout deposits calculated from the isopach data shown in Table 4 and their respective maximum thickness (T_{max}); slope coefficient (k), R-squared value (R) and volume (V) calculated from the plot shown in Fig. 8 (after Pyle, 1989, 1995)

Layer	T (cm)	A (km^2)	T_{max} (cm)	k	R^2	V (km^3)
A	55	1				
A	25	18				
A	20	37				
A	15	67				
A	10	105				
A	5	192				
A	1	576				
A	–	–	57.997	−0.1713	0.9962	0.040
C	26	1				
C	15	31				
C	10	94				
C	5	286				
C	1	1089				
C	–	–	27.285	−0.1005	0.9992	0.054
E	22	1				
E	15	52				
E	10	145				
E	5	624				
E	1	2500				
E	–	–	22.979	−0.0626	0.9985	0.117
F	68	1				
F	45	19				
F	40	62				
F	35	94				
F	30	136				
F	25	204				
F	20	383				
F	15	617				
F	10	882				
F	5	1167				
F	1	3844				
F	–	–	68.632	−0.0685	0.9893	0.293
Vol H=Vol F=						0.293
C.P. main fallout deposits total volume:						0.796

T=1 cm is inferred.

4.15. Layer G (column collapse pumice fallout deposit)

Layer G is a 6-cm-thick, brown, massive and relatively compacted pumice fallout deposit (Figs. 2, 4 and 6) and Table 1). It mainly outcrops on the eastern flanks of the cone and was recognized up to a distance of over 30 km from the vent. The layer is constituted with fine, altered pumice, sub-angular andesitic clasts and fine loose crystals dispersed in the matrix. Layer G lower contact with Layer F is always very sharp due to the strong granulometry differences. Layer G was associated with the third resumed sustained column fallout deposit.

4.16. Layer 3 (vulcanian pumice-rich pf deposit)

Layer 3 is a max 2-m-thick (~50 m aside from the valley axis), dark-brown, massive and ungraded, matrix supported, pumice-rich pyroclastic flow deposit (Figs. 2,3 and 4 and Table 1). It outcrops in the narrow valleys running along the eastern and southeastern flanks of the volcano and is composed mainly of rounded and altered (reddish) andesitic (Fig. 5 and Table 2) pumice clasts; broken, gray, andesitic blocks; a few scattered black andesitic (Fig. 5 and Table 2) scoria bombs and fine matrix. Pumice clasts show rounded vesicles with a diameter up to 5 mm and with relatively thick inter-bubble walls. The clast size is highly variable (from lapilli to decimetric blocks) with the average around 20 cm in diameter. In the area of Teteltzingo (site 67) (Fig. 3) at one side of the river, the deposit sits in erosional contact on Layer F, but its lateral continuity varies from 30 cm (as in Fig. 4) up to a couple of meters within a few tens of meters. Such aspect suggests that the deposit was emplaced in a relatively horizontal but undulated area. Due to the thick tropical vegetation of the area, the lateral pinch-out of Layer 3 was not found. Layer 3 was associated with the second C.P. vulcanian phase.

4.17. Layer H (Plinian pumice fallout deposit)

Layer H is a 20-cm-thick gray-to-yellow, massive-to-normal graded, clast-supported pumice fallout deposit (Fig. 2, 4 and 6) and Table 1). It was found all around the cone, with major abundance towards the Eastern quadrants of the cone up to a distance of about 25 km (see isopach and isopleth curves below). It is composed of light-yellow angular basaltic–andesitic pumice (Fig. 5 and Table 2), gray, angular, andesitic clasts and

Table 4
Mean maximum layer thickness (averaged from three measures), mean maximum diameter of pumice and lithic clasts (averaged from five clasts) and UTM coordinates of each outcrop site shown in Fig. 1

Quadrant	Distance (km)	Site #	Mean maximum layer thickness (cm)							Mean maximum diameter										UTM Coordinates			Locality
										Pumice					Lithics					Long	Lat	Altitude (m a.s.l.)	
			A	C	E	F	E+F	H	Total	A	C	E	F	H	A	C	E	F	H	(14 Q UTM)			
N	4.6	91	0	0	0	0	0	0	0	0.0	0.0	0.0	0.0	0.0	0.0	0.0	0.0	0.0	0.0	681584	2109499	4005	N Hut
	5.1	92	0	0	<4	<8	<12	0	<12	0.0	0.0	2.0	3.0	0.0	0.0	0.0	3.2	4.6	0.0	680805	2109654	3980	N Pico
	5.5	93	0	0	3	7	10	0	10	0.0	0.0	2.1	2.0	0.0	0.0	0.0	3.2	4.5	0.0	680199	2109689	3937	N Pico
	5.8	73	–	–	–	–	–	–	–	–	–	–	–	–	–	–	–	–	–	683136	2110761	3900	Nueva Vaquería W
	6.4	98	0	0	7	20	27	0	27	0.0	0.0	2.2	3.2	0.0	0.0	0.0	2.8	4.4	0.0	681371	2110803	3734	N Pico
	6.5	99	0	<6	8	15	23	0	<29	0.0	4.2	2.2	3.5	0.0	0.0	3.5	2.5	4.2	0.0	681986	2111178	3809	N Pico
	6.8	74b	0	10	9	22	31	>30	>71	0.0	5.4	2.7	5.2	4.1	0.0	4.2	3.2	4.2	3.2	684653	2111210	3435	Pico NE
	7.0	100	0	0	5	10	15	0	15	0.0	0.0	2.0	3.0	0.0	0.0	0.0	3.2	4.4	0.0	679386	2110951	3715	N Pico
	7.2	97	0	0	<4	<6	<10	0	<10	0.0	0.0	1.5	2.0	0.0	0.0	0.0	3.1	4.2	0.0	679111	2110960	3668	N Pico
NE	8.0	72	9	9	9	20	29	>20	>67	0.0	5.2	2.9	4.0	3.3	0.0	4.1	2.6	3.6	3.0	686308	2111707	3279	Nueva Vaquería W
	8.2	85	9	9	8	20	28	0	46	0.0	5.2	3.0	4.0	0.0	0.0	4.3	2.8	3.5	0.0	685972	2112436	3262	W Nueva Vaquería
	8.6	86	9	9	8	20	28	0	46	0.0	4.6	2.5	3.9	0.0	0.0	3.8	2.6	3.8	0.0	686044	2112958	3169	W Nueva Vaquería
	9.1	55	9	9	8	20	28	>5	>51	0.0	4.4	2.6	4.1	2.8	0.0	3.2	2.7	3.6	2.2	686054	2113103	3130	El Jacal
	9.2	51	8	8	8	20	28	>5	>49	2.8	4.2	2.5	3.9	3.1	2.6	2.8	2.4	3.6	2.2	688203	2111888	3058	Nueva Vaquería
	10.0	84	8	8	8	19	27	0	43	0.0	4.1	3.3	3.8	0.0	0.0	3.2	4.0	3.5	0.0	688266	2112886	2941	W Nueva Vaquería
	11.1	54	–	–	–	–	–	–	–	–	–	–	–	–	–	–	–	–	–	688764	2114188	2800	Tlacotiopa
	12.0	52	–	–	–	–	–	–	–	–	–	–	–	–	–	–	–	–	–	689777	2114260	2680	Palo Gacho
	13.3	53	–	–	–	–	–	–	–	–	–	–	–	–	–	–	–	–	–	691345	2114909	2550	Dos Caminos
	13.6	83	–	–	–	–	–	–	–	–	–	–	–	–	–	–	–	–	–	691389	2114710	2544	Dos Caminos
	13.6	49	0	0	8	16	24	>5	>29	0.0	0.0	2.1	3.4	2.9	0.0	0.0	1.2	1.4	1.9	694464	2111041	2350	Malacatepec
	14.1	71	–	–	–	–	–	–	–	–	–	–	–	–	–	–	–	–	–	692273	2114694	2411	Tlicotiopa
	15.4	43	–	–	–	–	–	–	–	–	–	–	–	–	–	–	–	–	–	695968	2111766	2450	S Ayahualulco
	15.5	70	–	–	–	–	–	–	–	–	–	–	–	–	–	–	–	–	–	693481	2115550	2227	Tecoanapa
	16.4	46	–	–	–	–	–	–	–	–	–	–	–	–	–	–	–	–	–	696391	2113143	2310	Ayahualulco
	16.5	50	–	–	–	–	–	–	–	–	–	–	–	–	–	–	–	–	–	694366	2116102	2140	Excola
	16.6	50b	–	–	–	–	–	–	–	–	–	–	–	–	–	–	–	–	–	694419	2116146	2149	Excola
	16.8	44	0	0	8	12	20	0	20	0.0	0.0	0.7	1.4	0.0	0.0	0.0	0.4	0.4	0.0	697098	2112838	2250	Ayahualulco E
	17.2	5	–	–	–	–	–	–	–	–	–	–	–	–	–	–	–	–	–	695073	2116319	2150	Excola
	17.4	69	0	0	8	11	19	0	19	0.0	0.0	0.6	1.7	0.0	0.0	0.0	0.5	0.4	0.0	697621	2112761	2190	Ayahualulco E
	17.9	57	–	–	–	–	–	–	–	–	–	–	–	–	–	–	–	–	–	693304	2118828	2080	NW Excola
	18.1	42	–	–	–	–	–	–	–	–	–	–	–	–	–	–	–	–	–	698201	2113010	2040	Ayahualulco E
	19.0	41	–	–	–	–	–	–	–	–	–	–	–	–	–	–	–	–	–	698981	2113453	1860	Ayahualulco E
E	6.8	32	10	12	15	42	57	>15	>94	5.2	6.2	3.1	6.2	5.7	4.4	4.5	3.2	4.6	5.2	689086	2105062	3133	La Paloma
	8.2	31	–	–	–	–	–	–	–	–	–	–	–	–	–	–	–	–	–	690268	2103874	2880	La Mata
	8.8	76	9	8	11	35	46	>15	>78	4.2	5.1	2.9	5.1	4.7	3.9	4.2	2.4	4.2	5.0	690993	2105743	3061	Cuyachapa SW
	9.7	28	0	0	12	35	47	>20	>67	0.0	0.0	3.1	4.2	3.5	0.0	0.0	2.5	3.6	4.1	691670	2102107	2524	Naranjillos W
	9.8	30	9	6	10	35	45	>20	>80	3.4	4.6	2.9	4.1	3.4	3.0	4.0	2.4	3.6	4.1	691805	2102565	2600	Naranjillos N

(continued on next page)

Table 4 (*continued*)

Quadrant	Distance (km)	Site #	Mean maximum layer thickness (cm)							Mean maximum diameter										UTM Coordinates			Locality
										Pumice					Lithics					Long	Lat	Altitude (m a.s.l.)	
			A	C	E	F	E+F	H	Total	A	C	E	F	H	A	C	E	F	H	(14 Q UTM)			
	10.0	75	9	8	9	34	43	>10	>70	3.4	4.7	2.7	4.2	3.6	3.2	4.1	2.2	3.7	3.2	692304	2104837	2874	Cuyachapa W
	10.5	29	–	–	–	–	–	–	–	–	–	–	–	–	–	–	–	–	–	692075	2101779	2549	Naranjillos
	11.2	35	8	6	8	25	33	>20	>67	3.1	4.1	2.6	3.6	3.3	1.9	3.2	2.2	3.5	3.2	693442	2106424	2570	Cuiyachapa E
	12.0	34	0	0	8	21	29	0	29	0.0	0.0	2.4	3.5	0.0	0.0	0.0	2.3	3.2	0.0	693900	2108169	2490	El Potrerillo
	12.2	36	0	0	8	>22	>30	0	>30	0.0	0.0	2.5	3.6	0.0	0.0	0.0	1.9	3.2	0.0	694475	2105950	2519	Teteltzingo S
	12.3	37	0	0	8	25	33	0	33	0.0	0.0	2.7	3.7	0.0	0.0	0.0	1.8	3.1	0.0	694536	2103953	2280	Tenixtepec
	12.5	66	0	0	9	20	29	0	29	0.0	0.0	2.5	3.5	0.0	0.0	0.0	2.1	3.2	0.0	694297	2108319	2440	Teteltzingo-Cuyachap
	12.8	67	3	5	9	20	29	>5	>42	2.4	3.4	2.7	3.3	3.4	1.4	2.8	1.4	3.1	2.4	694887	2107919	2395	Teteltzingo-Cuyachap
	13.8	6	0	5	8	18	26	>4	>35	0.0	3.5	1.6	3.4	3.3	0.0	2.8	0.8	2.6	2.0	695619	2108064	2390	Teteltzingo
	16.2	48	–	–	–	–	–	–	–	–	–	–	–	–	–	–	–	–	–	697308	2110618	2140	Ayahualulco S
	16.9	47	–	–	–	–	–	–	–	–	–	–	–	–	–	–	–	–	–	697868	2111458	2100	Ayahualulco S
	22.8	39	–	–	–	–	–	–	–	–	–	–	–	–	–	–	–	–	–	704352	2100656	1530	Tetla
	24.8	40	0	0	<2	<10	<12	0	<12	0.0	0.0	0.4	0.8	0.0	0.0	0.0	0.3	0.6	0.0	706946	2102743	1370	Chocamán
SE	4.8	4	–	–	–	–	–	–	–	–	–	–	–	–	–	–	–	–	–	686664	2102381	3610	Rancho Nuevo W
	5.6	9	23	>4	9	45	54	>20	>101	5.3	6.2	3.7	6.8	5.7	4.7	4.7	4.1	4.7	5.3	686203	2102024	3410	Rancho Nuevo W
	6.0	88	–	–	–	–	–	–	–	–	–	–	–	–	–	–	–	–	–	687297	2100857	3234	Chinela
	6.5	89	17	11	12	42	54	>30	>110	4.6	5.6	3.0	6.3	5.2	4.3	4.3	2.7	4.3	4.6	687689	2101777	3364	SE Pico
	6.5	8	19	12	9	42	51	>30	>112	4.6	5.1	2.8	6.2	5.2	4.2	4.2	2.4	4.2	4.7	686317	2099453	3251	Pilancón SE
	6.8	7	19	12	10	42	52	25	108	4.4	5.2	2.8	6.2	5.1	4.2	4.3	2.4	4.2	4.6	686842	2099723	3228	Pilancón
	7.9	3	18	10	9	37	46	>18	>92	4.2	5.2	3.0	5.9	4.5	3.5	4.1	2.2	4.0	4.2	688086	2099391	2997	Pilancón E
	8.0	77	0	8	10	28	38	>55	>101	0.0	4.2	3.1	6.2	4.4	0.0	3.1	3.2	3.9	3.2	685310	2097608	2971	Texmola N
	8.8	87	15	8	9	>35	>44	>27	>94	3.8	4.5	2.8	5.3	4.2	2.2	3.3	2.4	3.7	2.4	688732	2098854	2858	S Chinela
	9.2	13	15	9	9	>35	>44	0	>68	3.5	4.3	2.2	5.2	0.0	2.1	2.8	2.0	3.6	0.0	689327	2098937	2742	Agua Escondida
	9.4	2	13	9	9	>35	>44	0	>66	3.6	4.3	2.2	4.2	0.0	2.1	2.2	1.9	3.6	0.0	689822	2098937	2682	Agua Escondida E
	9.9	12	0	9	?	?	?	0	?	0.0	4.0	?	?	0.0	0.0	2.2	?	?	0.0	690093	2098744	1196	Xometla
	10.4	65	0	8	8	32	40	0	48	0.0	4.1	1.9	4.2	0.0	0.0	2.2	2.1	3.5	0.0	690714	2098971	2610	Xometla
	11.8	17	–	–	–	–	–	–	–	–	–	–	–	–	–	–	–	–	–	686885	2094235	2660	Loma Grande
	12.2	11b	0	0	8	>30	>38	0	>38	0.0	0.0	3.0	3.8	0.0	0.0	0.0	1.8	3.2	0.0	692496	2098096	2417	El Lindero N
	12.6	11	–	–	–	–	–	–	–	–	–	–	–	–	–	–	–	–	–	692587	2097922	2379	El Lindero N
	13.1	10	–	–	–	–	–	–	–	–	–	–	–	–	–	–	–	–	–	693097	2097601	2260	El Lindero S
	13.4	18	0	0	9	>15	>24	0	>24	0.0	0.0	3.0	3.7	0.0	0.0	0.0	2.8	3.0	0.0	689766	2093572	2550	San Isidro Berro
	14.4	26	–	–	–	–	–	–	–	–	–	–	–	–	–	–	–	–	–	695014	2098607	2160	Cumbre del Español
	14.8	27	–	–	–	–	–	–	–	–	–	–	–	–	–	–	–	–	–	633266	2099575	2180	Cumbre del Español
	15.4	33	0	0	9	21	30	>10	>40	0.0	0.0	2.2	2.6	2.9	0.0	0.0	0.8	2.7	1.9	695631	2097170	2533	El Zapote
S	7.6	108	0	0	>4	>9	>13	0	>13	0.0	0.0	5.5	5.8	0.0	0.0	0.0	4.6	3.8	0.0	681594	2097417	3302	N Texmalaquilla
	9.5	20	0	0	>5	>15	>20	0	>20	0.0	0.0	2.9	4.7	0.0	0.0	0.0	2.8	3.0	0.0	680840	2095627	3200	Texmalaquilla
	9.6	14	0	5	8	25	33	>15	>53	0.0	3.8	3.0	4.8	4.2	0.0	1.8	3.0	3.7	1.9	685009	2095884	2915	Texmola N
	10.0	24	0	0	11	22	33	21	54	0.0	0.0	2.7	4.2	1.8	0.0	0.0	2.6	2.8	1.6	680395	2095274	3100	Texmalaquilla
	10.6	19	–	–	–	–	–	–	–	–	–	–	–	–	–	–	–	–	–	–	–	–	–
	11.0	90	2	0	9	>12	>21	0	>23	0.0	0.0	3.0	4.5	0.0	0.0	0.0	2.9	3.5	0.0	685140	2094861	2845	Texmola

	11.8	16	0	0	9	>15	>24	0	>24	0.0	0.0	2.9	4.2	0.0	0.0	0.0	2.8	3.1	0.0	686401	2093543	2690	Loma Grande
	12.3	25	0	0	?	?	?	0	?	0.0	0.0	2.7	4.3	0.0	0.0	0.0	2.8	2.8	0.0	684281	2092812	2708	Paso Carretas
	14.8	107	0	0	0	0	0	0	0	0.0	0.0	0.0	0.0	0.0	0.0	0.0	0.0	0.0	0.0	677734	2091127	2752	Texmalaquilla
	16.0	1	0	0	0	0	0	0	0	0.0	0.0	0.0	0.0	0.0	0.0	0.0	0.0	0.0	0.0	676918	2090266	2680	Atzitzintla
	16.8	15	0	0	8	20	28	0	28	0.0	0.0	2.1	3.4	0.0	0.0	0.0	1.8	1.9	0.0	688292	2089056	2240	Sierra de Agua
	24.0	78	0	0	0	2	2	0	2	0.0	0.0	0.0	1.0	0.0	0.0	0.0	0.0	0.3	0.0	686643	2081608	1500	Maltrata
SW	5.1	23	–	–	–	–	–	–	–	–	–	–	–	–	–	–	–	–	–	679900	2100325	3950	Sierra Negra
	5.2	22	–	–	–	–	–	–	–	–	–	–	–	–	–	–	–	–	–	678817	2100923	4030	Sierra Negra
	5.3	21	–	–	–	–	–	–	–	–	–	–	–	–	–	–	–	–	–	679382	2100187	3960	Sierra Negra
W	8.9	104	0	0	0	0	0	0	0	0.0	0.0	0.0	0.0	0.0	0.0	0.0	0.0	0.0	0.0	674139	2108385	3097	Llano Grande
	9.5	103	0	0	0	0	0	0	0	0.0	0.0	0.0	0.0	0.0	0.0	0.0	0.0	0.0	0.0	673076	2106762	3051	Llano Grande
	12.8	105	0	0	0	0	0	0	0	0.0	0.0	0.0	0.0	0.0	0.0	0.0	0.0	0.0	0.0	670239	2108944	2871	S.M. El Aserradero
	14.0	106	0	0	0	0	0	0	0	0.0	0.0	0.0	0.0	0.0	0.0	0.0	0.0	0.0	0.0	669353	2110112	2813	Ávalos
	18.5	58	0	0	0	0	0	0	0	0.0	0.0	0.0	0.0	0.0	0.0	0.0	0.0	0.0	0.0	664525	2099811	2600	Cd Serdán
NW	6.1	82	0	0	10	15	25	0	25	0.0	0.0	2.1	5.2	0.0	0.0	0.0	3.3	4.3	0.0	679598	2110022	3908	E Miguel Hidalgo
	6.5	81	0	<6	9	14	23	0	<29	0.0	3.2	1.7	5.3	0.0	0.0	3.4	3.1	4.2	0.0	679400	2110459	3842	E Miguel Hidalgo
	6.8	80	0	0	8	0	8	0	8	0.0	0.0	1.5	0.0	0.0	0.0	0.0	2.9	0.0	0.0	678684	2110702	3840	E Miguel Hidalgo
	6.9	61	0	0	0	0	0	0	0	0.0	0.0	0.0	0.0	0.0	0.0	0.0	0.0	0.0	0.0	677659	2110039	3400	Miguel Hidalgo
	7.1	94	0	0	<5	<6	<11	0	<11	0.0	0.0	1.6	3.0	0.0	0.0	0.0	3.1	4.0	0.0	678708	2110945	3720	N Pico
	7.1	60	0	0	0	0	0	0	0	0.0	0.0	0.0	0.0	0.0	0.0	0.0	0.0	0.0	0.0	677135	2109882	3383	Miguel Hidalgo
	7.2	63	0	0	0	0	0	0	0	0.0	0.0	0.0	0.0	0.0	0.0	0.0	0.0	0.0	0.0	677285	2110304	3430	Miguel Hidalgo
	7.6	62	0	0	0	0	0	0	0	0.0	0.0	0.0	0.0	0.0	0.0	0.0	0.0	0.0	0.0	677642	2110987	3518	Miguel Hidalgo
	7.8	96	0	0	0	0	0	0	0	0.0	0.0	0.0	0.0	0.0	0.0	0.0	0.0	0.0	0.0	678418	2111448	3617	N Pico
	7.9	95	0	0	0	0	0	0	0	0.0	0.0	0.0	0.0	0.0	0.0	0.0	0.0	0.0	0.0	678352	2111403	3639	N Pico
	8.8	101	0	0	0	0	0	0	0	0.0	0.0	0.0	0.0	0.0	0.0	0.0	0.0	0.0	0.0	677670	2111719	3582	NE Miguel Hidalgo
	9.0	102	0	0	0	0	0	0	0	0.0	0.0	0.0	0.0	0.0	0.0	0.0	0.0	0.0	0.0	675131	2109875	3171	Zoapan
	10.1	78	0	0	0	0	0	0	0	0.0	0.0	0.0	0.0	0.0	0.0	0.0	0.0	0.0	0.0	676597	2113487	3236	Puerto Nacional
	10.2	59	0	0	0	0	0	0	0	0.0	0.0	0.0	0.0	0.0	0.0	0.0	0.0	0.0	0.0	673406	2110357	2981	Zoapan
	10.4	79	0	0	0	0	0	0	0	0.0	0.0	0.0	0.0	0.0	0.0	0.0	0.0	0.0	0.0	677230	2114149	3157	N Cajón
	13.0	64	0	0	0	0	0	0	0	0.0	0.0	0.0	0.0	0.0	0.0	0.0	0.0	0.0	0.0	670344	2110491	2799	Tlachichuca

Data were used to draw the isopachs and isopleths shown in Figs. 7, 9A and B, respectively.

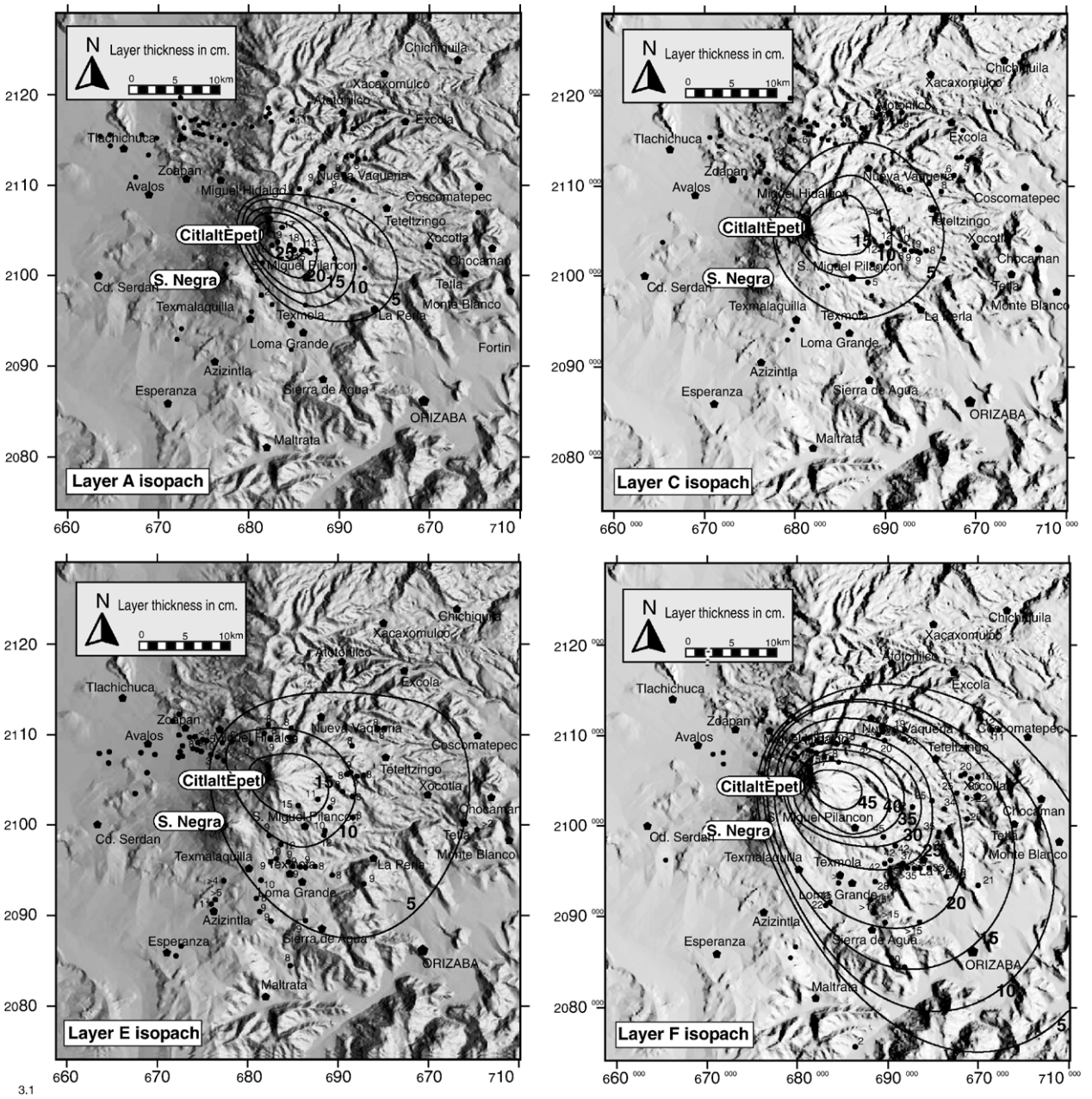

Fig. 7. Isopach maps for layers A, C, E and F and their respective sampling sites. Cities and towns are represented by pentagons. Numbers are in centimeters.

fine loose crystals scattered in the rare matrix. Pumice clasts show sub-elongated vesicles with a diameter up to 6 mm and with relatively thin inter-bubble walls. Layer H lower contact is sharp with Layer G or with the Layer 3 deposit in the Teteltzingo area, whereas the upper part of the layer, if the Layer 3 deposit is missing, is grading into the thick, sequence topmost soil. Layer H was associated with the fourth C.P. Plinian phase.

4.18. Layer S3 (proximal pumice-rich surge deposit)

Layer S3 is a 3-cm-thick, gray, clast supported, laminated pumice-rich horizon (Figs. 2 and 6 and Table 1). It is present around the cone and it was recognized only at a distance closer than 10 km from the vent. It is composed of lapilli-sized, clear and relatively dense pumice; angular, gray andesitic clasts and loose

Table 5
Physical eruption parameters of the different Citlaltépetl Pumice fallout layers

Parameter	Symbol	Formula used	Unit	Main fallout layer						
				A	C	E	F	H	Total	Ref.
Column bearing (isopach)	Azimuth	Picture extrapolation	deg	119	82	111	132	92	*	2
Layer thickness at vent distance=0.1 km	T_{max}	Plot extrapolation	m	58.00	27.29	22.98	68.63	68.63*		1
Slope coefficient	k	Plot extrapolation	–	−0.171	−0.101	0.063	−0.069	−0.069 *		1
Volume ejected	V	(Pyle, 1989)	km^3	0.040	0.054	0.117	0.293	0.293 *	0.796	1
Column bearing (isopleth)	Azimuth	Picture extrapolation	deg	88	83	137	123	92		2
Column height	H	Plot extrapolation	km	23	25	24	28	26		7
Mass discharge rate (intensity)	MDR	plot extrapolation	kg/s	3.00E+07	1.00E+08	5.00E+07	3.00E+08	2.00E+08		4
Layer bulk density	D_t	field measure	kg/m^3	620	680	860	650	630		2
Deposit mass (layer weight) (magnitude)	M_t	$V*D_t$	kg	2.45E+10	3.67E+10	1.01E+11	1.90E+11	1.84E+11*	5.36E+11	2
Eruption duration	Ed	M_t/MDR	s	816	367	2018	634	921*	4756	5
Juvenile clasts density	D_m	Lab measure	kg/m^3	867	653	872	975	897		2
Accessory lithics density	D_a	Inferred	kg/m^3	2600	2600	2600	2600	2600		2
Juvenile DRE	DRE_m	Lab measure	kg/m^3	2522	2401	2453	2618	2490		2
Accessory lithics DRE	DRE_a	Inferred	kg/m^3	2600	2600	2600	2600	2600		2
Magma weight (M_m)	M_m	M_t–M_a	kg	1.55E+10	2.36E+10	4.04E+10	1.35E+11	1.17E+11*	3.32E+11	3
Accessory lithics weight (M_a)	M_a	(M_t/100)*LTH%	kg	8.23E+09	1.23E+10	5.62E+10	5.32E+10	6.56E+10*	1.96E+11	2
Volume juvenile DRE_m	$VDRE_m$	M_m/D_m	m^3	6.14E+06	9.85E+06	1.64E+07	5.16E+07	4.71E+07*	1.31E+08	3
Volume accessory lithics DRE_a	$VDRE_a$	M_m/D_a	m^3	5.95E+06	9.10E+06	1.55E+07	5.19E+07	4.51E+07*	1.28E+08	3
Total volume DRE	$VDRE_{tot}$	$VDRE_m$+ $VDRE_a$	m^3	1.21E+07	1.89E+07	3.20E+07	1.03E+08	9.21E+07*	2.59E+08	3
Accessry LTH content	LTH%	Lab measure	% (wt)	33.6	33.5	55.7	28.0	35.6		2
Magma PM content (M_m)	PM%	Lab measure	% (wt)	63.2	64.4	40.0	71.0	63.6		2
Volume (DRE) discharge rate	VDR	$VDRE_{tot}$/Ed	km^3/s	1.48E+04	5.16E+04	1.58E+04	1.63E+05	1.00E+05*		6

Key: PM=pumice; LTH=lithic clast; DRE=density rock equivalent; m=magma (juvenile); a=accessory lithic clasts (mainly andesite); *=value estimated; pi=3.14.
References: (1) Pyle (1989, 1995) and Fierstein and Nathenson (1992); (2) this work; (3) Rodríguez et al. (2002); (4) Wilson and Walker (1987); (5) Walker (1980); (6) Walker (1981); (7) Carey and Sparks (1986). Parameters are shown following the text order.

crystals dispersed in the rare matrix. This horizon is intercalated within Layer H and its lower and upper contacts are sharp due to sudden granulometric difference. Layer S3 was again associated with a third, inter-Plinian surge event recorded only at proximal vent distances.

4.19. Layer 4 (vulcanian pumice-rich pf deposit)

Layer 4 is a tens-of-centimeter-thick (variable thickness), dark-brown, massive and ungraded, matrix supported, pumice-rich pyroclastic flow deposit (Figs. 2 and 4 and Table 1). Contrary to the pyroclastic flow deposits described before, Layer 4 outcrops in different places in the SE flanks of the cone and not only into the narrow valleys (e.g., site 3 or site 34) (Figs. 1 and 3). These characteristics suggest that the flow associated with Layer 4 managed to spill out of the narrow gullies and spread around into the adjacent smooth but undulated plains. The deposit is constituted by fine matrix in which there are rounded and altered andesitic pumice (Fig. 5 and Table 2), broken, black, bread-crusted, cauliflower-shaped, andesitic scoria bombs

(Fig. 5 and Table 2) and gray, angular, andesitic clasts. Pumice clasts show rounded vesicles with a diameter up to 5 mm and with relatively thick inter-bubble walls. The clast size is very variable with an average of about 10 cm in diameter. The Layer 4 lower limit is in sharp erosional contact with Layers F, G or H and the upper limit fades into the gray-brown upper soil which closes the C.P. sequence. Due to its wide lateral speeding mentioned above, the Layer 4 lateral pinch-out was not found in the studied area. Layer 4 was associated with the third and last C.P. vulcanian phase.

5. Distribution and volumes of the Citlaltépetl pumice deposits

The thickness and the maximum clast diameter of each of the main fallout layers of the C.P. were measured in order to draw the isopach and isopoleth curves, respectively. Isopach curves data allowed to calculate the volume of each main fallout layer by using the method proposed by Pyle (1989, 1995) and by Fierstein and Nathenson (1992) (Table 3). From the isopleth curves data, and using the method proposed by Carey and Sparks (1986) the column height was finally determined.

5.1. Volume calculation for the C.P.

5.1.1. Isopach maps

In order to measure the maximum thickness of each layer, the three major layer thicknesses in each outcrop (sites in Fig. 1) were averaged to obtain the field mean maximum thickness of each outcrop as shown in Table 4.

Isopach curves for the key Layers A, C, E and F were then obtained (thickness of the Layer H isopach was underestimated due to the erosion of its topmost part). Isopachs for A, C, E and F show a clear east and southeastward preferential wind direction (Fig. 7).

Layers A and F isopachs have a general elongated shape to the SE (Table 5), with the 5-cm-thick curve reaching 16 km from the vent for Layer A and 36 km for Layer F. In contrast, Layers C and E isopachs show a more circular shape suggesting moderate wind

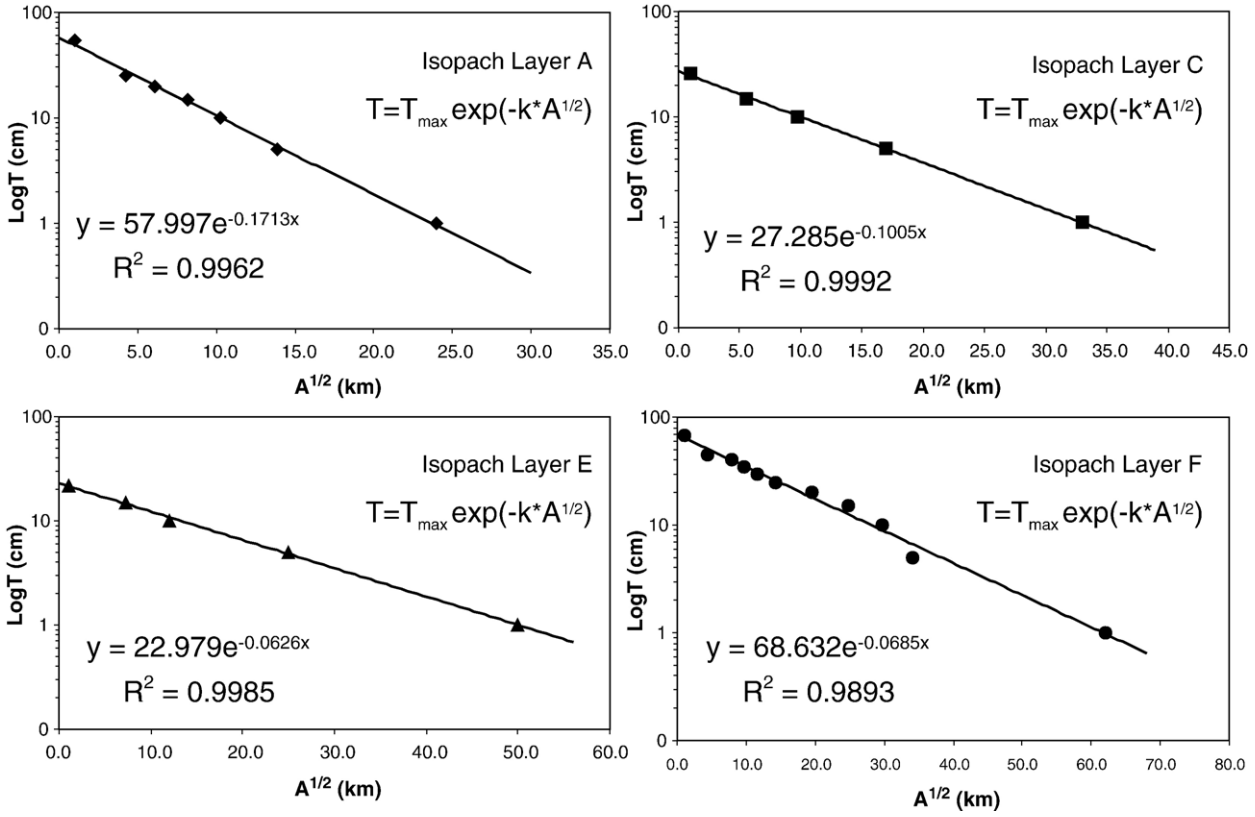

Fig. 8. Isopach logarithmic thickness (T) versus the square root of the isopach area (A) for the calculation of the A, C, E and F layers maximum thickness (T_{max}) and consequent volume according to the method proposed by Pyle (1989) and Fierstein and Nathenson (1992). Field data fit in a straight line where the slope coefficient (k) is the exponent of the line equation and T_{max} is the "e" coefficient. The lack of the distal data did not allow plotting the distal curve. See text for details.

influence, with the 5-cm-thick curve reaching 15 and 25 km from the vent, respectively (Fig. 7). Although the isopach measurements thinner than 5 cm were inferred (Table 3), they were not reported due to the stratigraphic uncertainties encountered in the distal areas of the volcano flanks.

5.1.2. Volume

Volumes of the C.P. fallout deposits were calculated using the "exponential thinning" method (Pyle, 1989, 1995; Fierstein and Nathenson, 1992). With the knowledge of the layer thickness (T) measured in the field for each layer (Table 4), and the area (A) of each isopach curve (Table 3) calculated as described below, it was possible to extrapolate the maximum layer thickness (T_{max}) at the vent in accordance with the following equation (Pyle, 1989):

$$T = T_{max}\exp(-k*A^{1/2})$$

where "k" is a slope coefficient mathematically calculated for each layer and plotted in Fig. 8.

T_{max} and k values obtained for the C.P. fallout deposits are shown in Tables 4 and 5. Due to field evidence of similarity in thickness, sorting, distribution, granulometry and components composition among the Layers F and H deposits, the Layer H T_{max} and k parameters were inferred to be similar to those in Layer F. The area of each isopach curve was calculated using a simple kilometric lattice method: a transparent slide with a scaled grid (one square = 1 km^2) printed on it was overlaid on each curve, and then the squares inside each iso-curve were manually counted. Once T_{max} was calculated for each layer, the values were used to calculate the respective layer volumes (V) in accordance with the following equation (Pyle, 1989):

$$V = 2*T_{max}/k^2$$

Volume calculation results for each layer are shown in Tables 4 and 5. The total volume of the C.P. fallout deposits is 0.80 km^3. This value, added to the pyroclastic flow deposits volume of 0.26 km^3 calculated by Carrasco-Núñez and Rose (1995), yielded a total C.P. volume of 1.7 km^3. Such a total volume values (and further related calculated data) should only be taken as indicative of the total magnitude of the sequence of events that produced the C.P. deposits since they are the sum of deposit volumes belonging to distinct and time-lagged volcanic events. In addition, the result represents a minimum value, since the distal ashy portion (inferred to be 0.58 km^3 using the empirical approximations proposed by Carey et al., 1995) was not considered due to its great uncertainty for lack of reliable distal field data. Results show good agreement for the proximal and medial distance if compared with results obtained with other more recent methods described in literature (e.g., Bonadonna et al., 1998; Bonadonna and Houghton, 2005).

6. Eruption parameters

6.1. Column height calculation

6.1.1. Isopleth maps

In each section shown in Fig. 1, a 0.5-m^2 horizontal surface was used from each layer to collect the five largest clasts for both pumice and lithic clasts following the method described in Sigurdsson et al. (1985) and Carey and Sigurdsson (1986). The largest axis of each of the five clasts was recorded, and the values averaged to obtain a mean maximum pumice diameter value (MPD) and a mean maximum lithic diameter (MLD) for each of the main C.P. fallout layers as shown in Table 4. The MPD and MLD for Layers A, C, E, F and H were then used to obtain the respective isopleth maps (Fig. 9A and B), which show a general east to southeastward preferential wind direction for both pumice and lithic clasts (Table 5). The area and general shape for the pumice and lithic isopleths is similar, with the only exception of Layer E lithic clasts isopleth showing a slight bifurcated trend (Fig. 9B) possibly due to the lack of data in the central part of the area and not to an actual bifurcated wind trend since each measured pumice fallout layer has been here considered as erupted by a single continuous Plinian event and therefore not interrupted by depositional gaps.

6.1.2. Column height

Column height was calculated using the "Maximum clast method," proposed by Carey and Sparks (1986), who thought of the analysis of the lithic isopleths shape (Fig. 9B). It is assumed that particles of a certain diameter and density tend to segregate from the edge of iso-energy "envelopes".

Field data for Layers A, C, E, F and H of the Citlaltépetl Pumice are compared with data from some historically well-studied or eye-witnessed eruptions for lithic clasts with a maximum diameter of 3.2 cm and with density of 2500 kg/m^3. Such a diameter is the most common size present in our outcrops and its plotted values (Fig. 10) fit the plots proposed by Carey and Sparks, 1986. In accordance with the plot shown in Fig. 10, the resulting column values are shown in Table 5,

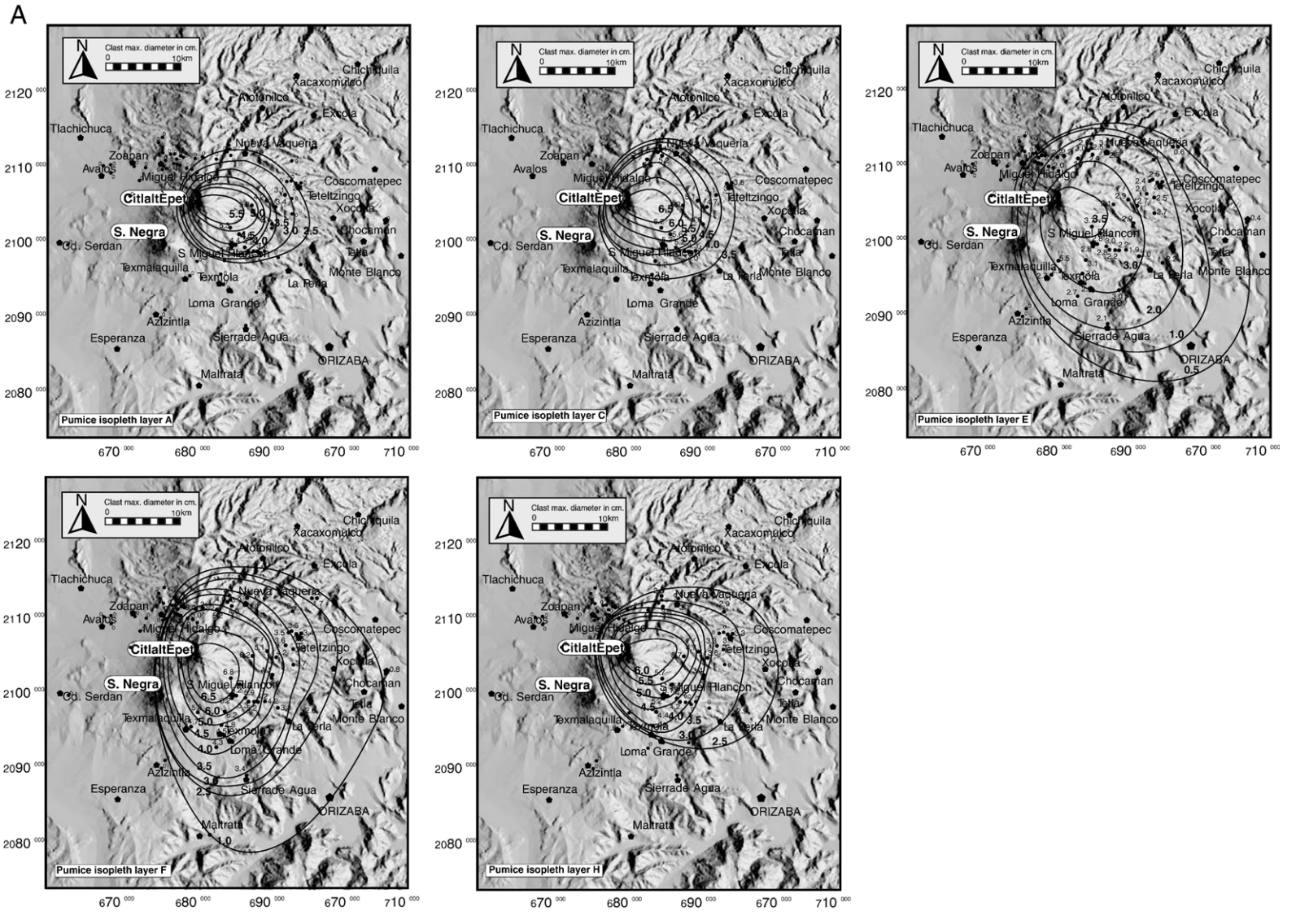

Fig. 9. Isopleth maps and sampling sites of (A) pumice clasts in layers A, C, E, F and H. (B) lithic clasts layers A, C, E, F and H. Cities and towns are represented by pentagons. Maximum thickness and diameter values for each studied outcrop (Fig. 1) are listed in Table 4.

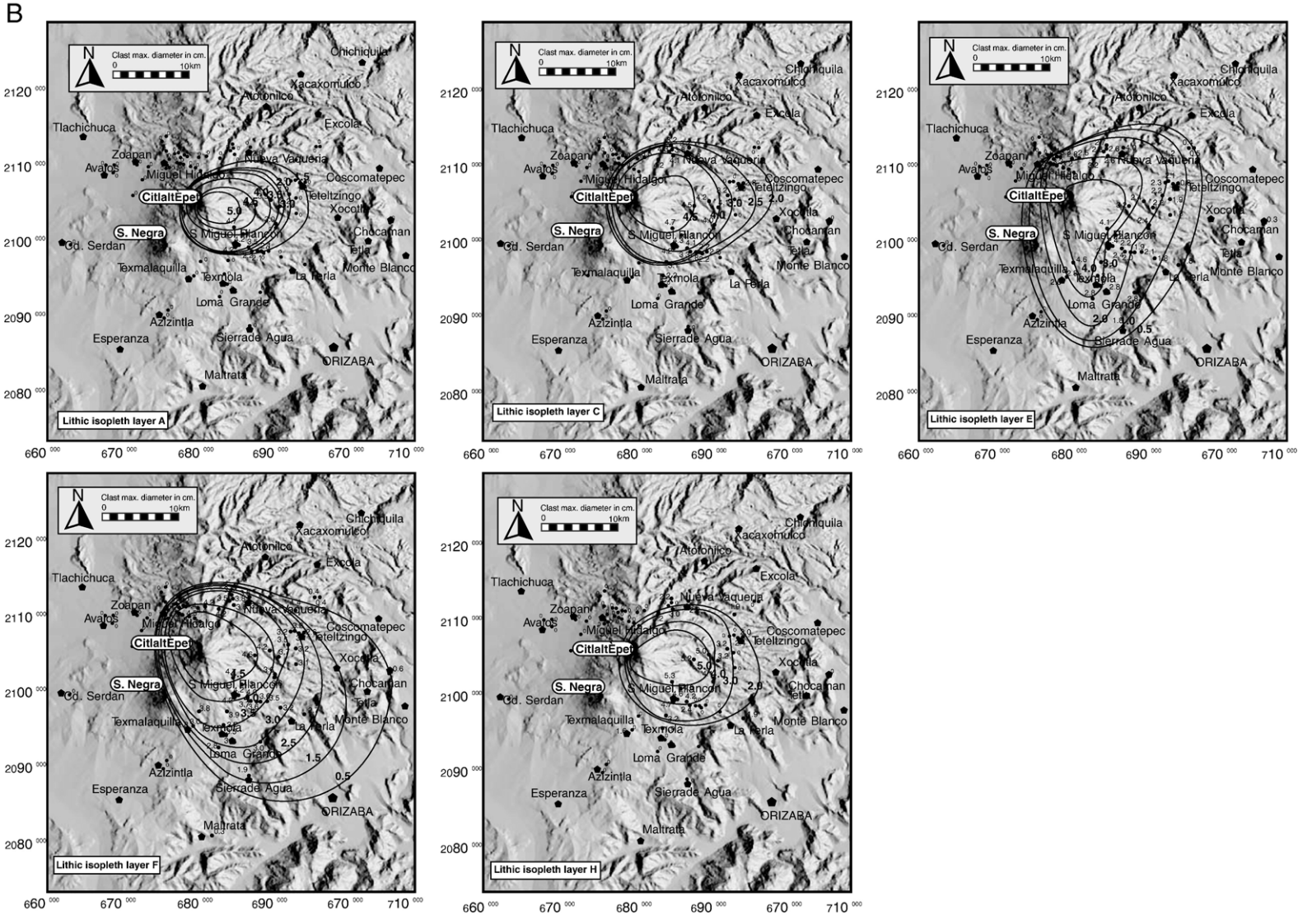

Fig. 9 (*continued*).

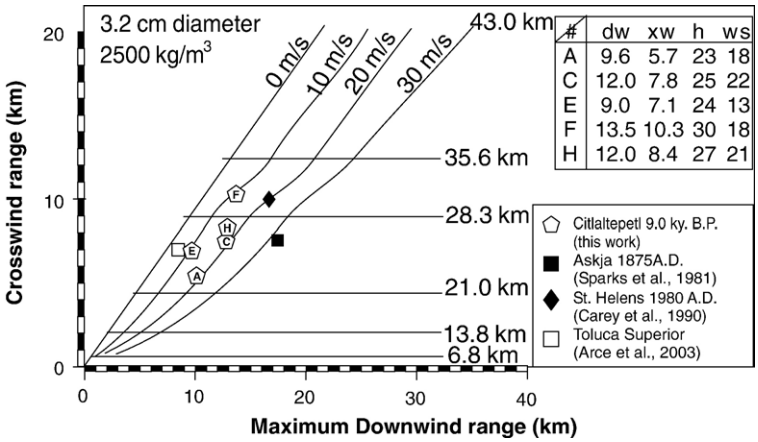

Fig. 10. Column height (h) calculation using the "Crosswind range (xw) versus maximum downwind range (dw) for 3.0 cm diameter lithic clasts" method proposed by Carey and Sparks (1986). C.P. column altitude results are compared with other eruptions data in literature (from Carey and Sparks, 1986). Diagonal lines represent wind speed (ws).

with, as suggested by the plot, a constant stratospheric wind ranging between 10 and 20 m/s. Such constant resulting values are consistent with the accepted definition of Plinian column (e.g., VEI by Newhall and Self, 1982) used in this paper.

6.2. Mass discharge rate (MDR)

The mass discharge rate (mass flux) (MDR) or eruption intensity is defined as the mass (kg) ejected from the vent during time unit (s) (Sparks, 1986; Wilson and Walker, 1987; Carey and Sigurdsson, 1989; Wilson and Hildreth, 1997) and, in addition to being one of the basic volcanic parameters to know when studying an eruption, it is the most important parameter for the calculation of the eruption duration, volume discharge rate and the column height. MDR for the C.P. was graphically determined by plotting the diameters of lithic clasts (d), their density (σ) and their respective cross-distance from the vent (D) into the "$d\sigma$ vs D" graph (Wilson and Walker, 1987) (Fig. 11).

In Table 5 the MDR values for each layer are shown.

6.3. Bulk density

Bulk density (D_t) for each layer was measured by tapping a sample of original tephra (pumice+lithic clasts) into a PVC container of known volume and then measuring its mass as described by Rodríguez et al. (2002). Measures were performed on three similar

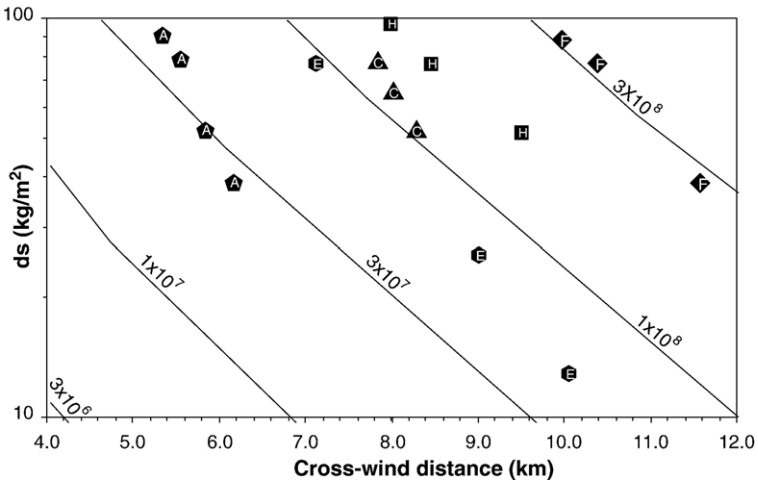

Fig. 11. Crosswind distance-from-vent versus diameter*density of the andesitic accessory lithic clasts (ds) plot. Calculation of the mass discharge rate (MDR) values [kg/s] for the eruptions associated to layers A, C, E, F and H, as proposed by Wilson and Walker (1987).

outcrops: site 3, 7.9 km SE from the vent; site 51, 9.2 km NE from the vent and site 75, 10 km N from the vent (Fig. 1). The results obtained were then averaged for each layer to obtain the bulk density values shown in Table 1 and 5. Layer E shows higher bulk density values due to its lithic-rich nature.

6.4. Eruption duration

Eruption duration (Ed) was calculated for each deposit according to the equation proposed by Walker (1980):

$$\mathrm{Ed} = M_t/\mathrm{MDR}$$

where M_t=total Plinian mass (bulk density * total volume ejected) (Table 5). Equation results suggest an eruption time of 14 min for the deposition of Layer A, 6 min for Layer C, 34 min for Layer E, 11 min for Layer F and 15 min for Layer H, for a total eruption time of 79 min (1.3 h) (Table 5). Such results should be understood as minimum values or as a strong underestimation of the actual eruption time since the proposed calculation does not take into account the volume of the thin horizons B, D, X, G, S1, S2 and S3 nor the volume of the distal fallout fines.

6.5. Juvenile and lithic clasts density

Density measurements of the single pumice clasts (D_m) were also performed on samples taken from each main fallout bed. Clast density varies with size up to a certain size value (e.g., Walker, 1981, or Rosi et al., 1999). According to Houghton and Wilson (1989), clasts ranging in size between 64 and 16 mm are large enough to have their density not changing if increasing the size and small enough to be easily treated with laboratory equipment. To calculate the density of the pumice clasts, 21 samples from each main fallout deposit (Layers A, C, E, F, H) and 17 samples from the four pyroclastic flow deposits (Layers 1, 2, 3, 4) were accurately cleaned from loose particles and dust with an ultrasonic method, dried at 80 °C for 24 h and then weighed on a two decimal digits lab scale. Vesiculated samples were then impermeabilized by multiple dipping in hot liquid paraffin (e.g., Houghton and Wilson, 1989) and their volume was then obtained by measuring the water displacement using a lab pycnometer (Barberi et al., 1989). The density values were then obtained dividing the sample mass by its volume. Averaged pumice density results for each layer are shown in Table 5 as well as for lithic clasts whose density was assumed to have the value of the andesite lava (2600 kg/m^3).

6.6. Density rock equivalent (DRE)

In order to calculate the pumice DRE and consequent vesicularity values obtained by the relationship among DRE and density, 6 pumice samples from each layer, after being carefully cleaned and dried, were pulverized at 50 μm and pressed into a cylinder of known diameter for 30 s at 30 tons/cm^2 with a "Graseby SPECAC AUTOPRESS" at UNAM-LUGIS 527 laboratory. The thickness of the cylinder, multiplied by its diameter and mass, yielded to the DRE since the vesicularity of the pumice clast obtained with the compression should be nearly zero. DRE for lithic clasts was assumed to be the same value as the lithic density (2600 kg/m^3). DRE averaged values for each main fallout and pyroclastic flow deposits show good agreement with the DRE values of the magma expected in accordance to its chemistry (Table 1).

6.7. DRE volume (VDRE) and volume discharge rate (VDR)

The volume DRE of a layer is defined as the ratio between its total mass over its component density. Values of juvenile and accessory mass and the correspondent VDRE for each fallout layer are shown in Table 5. Such a value is useful for calculating the VDR, which is defined as the DRE volume ejected from the vent during a time unit (Walker, 1981). VDR minimum values for the C.P. main fallout layers are also shown in Table 5. In order to show the trend and fitting of our results, we plotted them in a column height versus VDR plot (Fig. 12), together with other data of explosive eruptions existing in the literature (Wilson et al., 1978).

7. Reconstruction of the C.P. erupting history

Between 8.5 and 9.0 ky B.P., Citlaltépetl volcano was awakened by a very fluctuating eruptive style which included the production of pumice fallout alternated with pyroclastic flow deposits. Based on stratigraphic field and laboratory observations and supported by radiocarbon dating constraints (Rossotti and Carrasco-Núñez, 2004), we propose hereby an interpretative reconstruction of the entire C.P. (Fig. 13).

7.1. Pre-eruptive phreatic phase

A phreatic explosion marked the first Holocene awakening of the Citlaltépetl volcano. The involvement of external water during this initial phase is demonstrated by the abundance of sharp-edged, highly

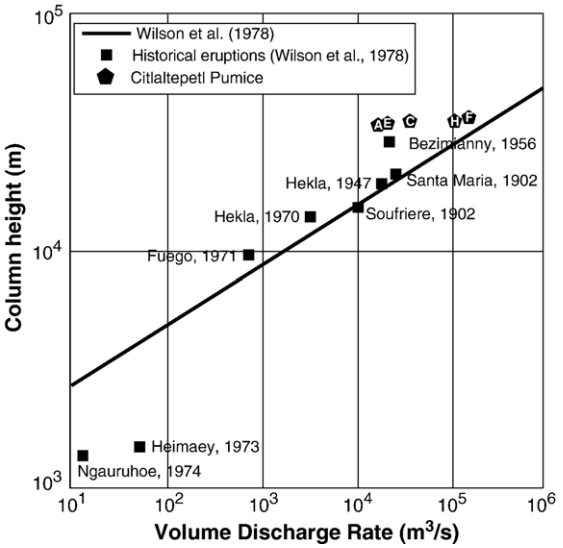

Fig. 12. Column height versus volume discharge rate plot. The solid diagonal lines represent the theoretical trend proposed by Wilson et al. (1978). Squares represent historical eruptions (from Wilson et al., 1978) and pentagons represent the values calculated here for the Citlaltépetl Pumice.

fragmented lithic clasts, abundance of free crystals in the finer fraction and the almost complete lack of juvenile fraction found in the deposit (Layer A0). It was inferred that this phase was the result of the first explosive pulse that unplugged the preexisting conduit as reported in other volcanoes such as Mount Vesuvius (Barberi et al., 1989); Nevado de Ruiz in 1985 (Barberi et al., 1990); the Holocene Plinian eruption of La Virgen volcano (Capra et al., 1997); the eruption of El Chichón (1982) or the Mt. St. Helens (1980) (Cioni et al., 2000), although juvenile clasts have been identified in the ash erupted by Mt. St. Helens during its "phreatic" phase that accompanied the May 18th activity (Cashman and Hoblitt, 2004).

7.2. First eruption (first vulcanian activity)

The vulcanian activity has been described for the first time by Mercalli (1906) for the 1888–1890 activity of Vulcano volcano in Italy. The vulcanian activity is characterized by the production of bread-crusted bombs and "cauliflower" scoria associated with a sequence of multiple short-lived explosions separated by intervals of several seconds to several hours, with a mass discharge ranging between 105 and 109 kg for each explosion and a maximum muzzle velocity of 400 m/s (e.g., Soufrière Hills volcano, Formenti et al., 2003). The first eruption of the Citlaltépetl Pumice, was represented by an intense and pulsating activity associated with the emplacement of a meter-thick, black, "cauliflower"-shaped scoria and bread-crusted bombs-bearing scoria flow deposit (Layer 1). Due to the similarity encountered with the activity described by Mercalli (1906), we consider the first C.P. activity as vulcanian. Since the distribution of the "cauliflower"-shaped and bread-crusted scoria clasts found in the pyroclastic flow is widely spread around the cone, they are interpreted as cognate clasts coming from a previous small andesitic dome grown in the summit crater. This vulcanian-driven scoria and pumice flow is considered as the first main explosive phase belonging to the C.P. sequence. Such activity was responsible for the devastation of an old forest, since abundant carbonized large tree trunks were found at the base of the deposit. Small localized lahar deposits found at the top of the Layer 1 (Rossotti and Carrasco-Núñez, 2004) were associated with the emplacement of the same flow and suggest a short period of repose during their formation.

7.3. Second eruption (first Plinian phase and partial column collapse)

The formation of a 23-km-high Plinian column and the associated pumice fallout deposit (Layer A) marked the onset of the second C.P. eruption. Such a Plinian eruption, as well as the other described hereafter, are possibly explained with the injection of hot magma into the magmatic chamber, which increased the internal system energy and triggered the Plinian eruption. A minor fluctuation of the Plinian phase, possibly due to the decline of the supply rate from the chamber induced by the volatile content waning (Bursik, 1993), is represented by a very thin ash layer interbedded in the main Layer A (Layer S1) and observed only at proximal facies (Figs. 13 and 2). A similar sequence was observed and explained in the same way for the pumice fallout deposits belonging to the ~1359 A.D. sub-Plinian eruption of Mono Lake volcanic complex (Bursik, 1993). After the paroxysm, the column waned, permitting the deposition of the thinner products as suggested by the deposition of Layer B which, for this reason, was interpreted as a result of a partial column collapse. Also, the slight alteration detected in this layer may suggest a brief period of repose.

7.4. Third eruption (second Plinian phase and main hiatus)

Although smaller in magnitude compared to the first one, the second Plinian phase was more intense (higher mass discharge rate). This event is related to the creation

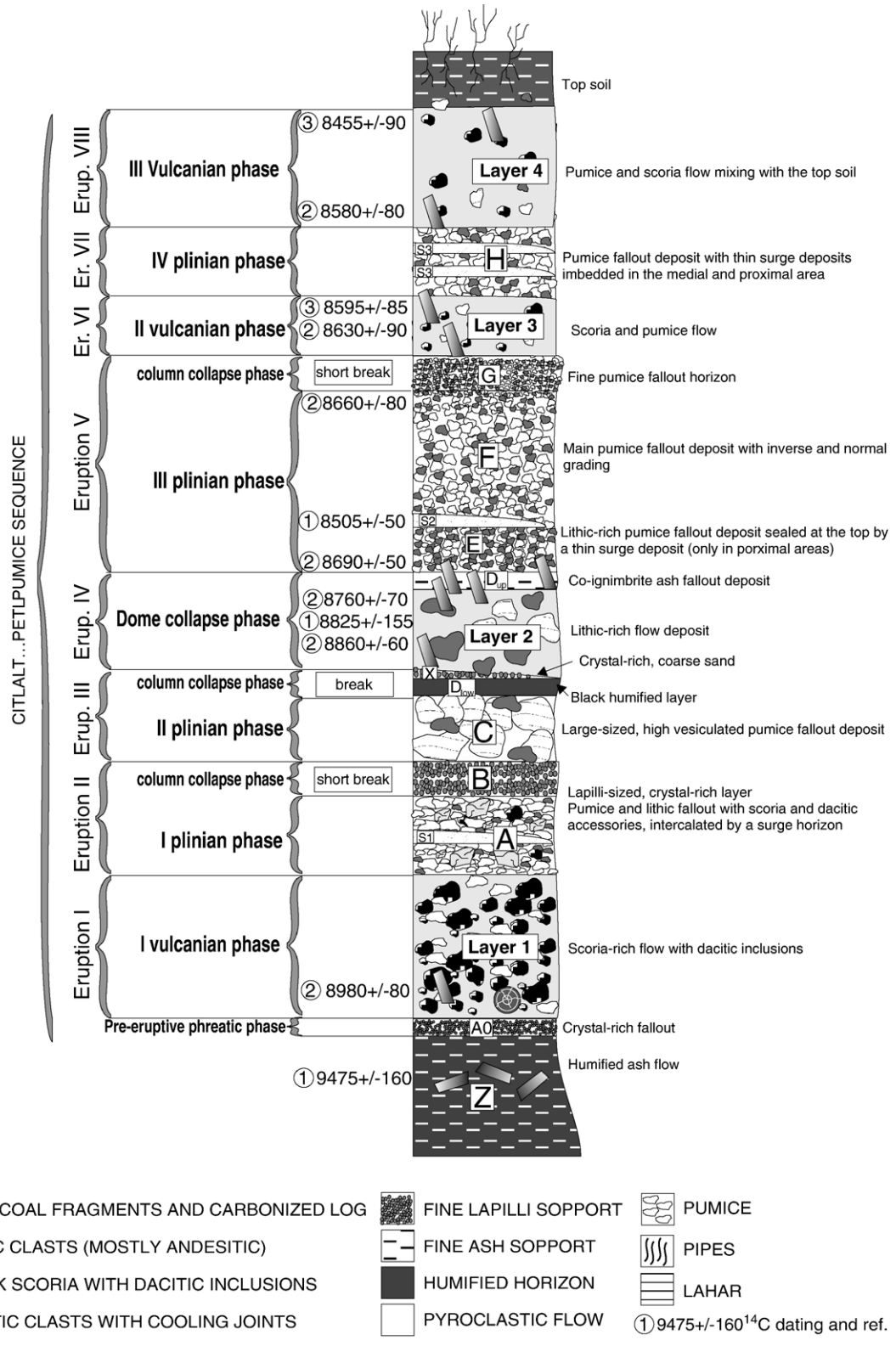

Fig. 13. Composite stratigraphic column representing the complete Citlaltépetl Pumice sequence. See text for further details. Radiocarbon dating: 1=Rossotti and Carrasco-Núñez (2004); 2=Carrasco-Núñez and Rose (1995); 3=Heine (personal communication, 1992).

of a column of about 25 km high suggested by the deposition of Layer C and it ends with a partial column collapse shown by the deposition of two thin layers of ash and lapilli (Layers D_{low} and X). Activity shows to have a marked repose break since Layer D_{low} shows an incipient soil development with some organic matter in it and Layer X is clearly reworked.

7.5. Fourth eruption (dome collapse phase)

After the main eruptive repose, an eruption of an andesitic magma produced a dense lithic-rich pyroclastic flow (Layer 2) emplaced in topographic depressions mainly near the villages of Tlachichuca and Teteltzingo (sites 25, 64 and 67) (Fig. 3). The monolithologic nature of this deposit suggests that the flow was formed due to the destruction of a small dome. The erupting mechanism was possibly a "boiling-over" activity (Wolf, 1878) due to the high density of the flow, as proposed by Carrasco-Núñez and Rose (1995). Due to its lithology and fading contact with Layer 2, a centimeter-scale fine ash horizon found in topographic heights has been associated with the lithic-rich pyroclastic flow as a co-ignimbrite deposit (Layer D_{up}), in a similar way as for layer UAB of the 1600 A.D. eruption of Huaynaputina volcano (Adams et al., 2001) or for layer F-5 in the 1815 Tambora eruption (Sigurdsson and Carey, 1989).

7.6. Fifth eruption (third Plinian phase and its partial column collapse)

The beginning of this phase produced a 23-km-high column (Layer E) that increased its intensity and reached the paroxysm, forming a 28-km-high Plinian column (Layer F). During the transition between the first and the second part, a small, nearly instantaneous partial collapse of the column occurred, producing a dune-bedded, pumice-rich surge-like layer only at proximal facies (run out less than 10 km from the vent) (Layer S2), described also for Layer S1 or for the eruption of Sao Miguel in Azores (Walker and Croasdale, 1970) or the 79 A.D. eruption of Mount Vesuvius (Carey and Sigurdsson, 1987). This transitional regime is also reported for Mt. St. Helens during its sub-Plinian pulsating phase (Scandone and Malone, 1985), for the sub-Plinian eruption of Mono Lake (Bursik, 1993) and theoretically simulated by Di Muro et al. (2004). In the Citlaltépetl pumice eruption, such a pulsating activity can explain the formation of small proximal surges before the emplacement of the steady Plinian column (S layers). As for the second eruption, the end of the paroxistic Plinian phase is also associated with the waning of the column and suggested by the deposition of a thin ashy pumice layer (Layer G) which was interpreted also as a short eruptive repose.

7.7. Sixth eruption (second vulcanian phase)

After a time of repose, the activity resumed with the production of a "cauliflower"-shaped scoria flow emplaced in deep valleys carved through the SE cone flanks. Due to the similarity in composition of the associated deposit (Layer 3) with Layer 1 and also the presence of scattered bread-crusted scoria clasts in the lower part of it, we also classified this activity as vulcanian.

7.8. Seventh eruption (fourth Plinian phase)

A new eruption produced the high-magnitude fourth Plinian phase of the sequence, characterized by the formation of a 26-km-high column associated with the deposition of Layer H. As for the plume that formed Layer E+F, during the growth of this column, we noticed fluctuations in the activity. Such fluctuations allowed the proximal deposition of several (at least 4) thin, ashy cross-bedded horizons, which were interpreted as proximally local pyroclastic surge deposits (Layer S3) (Figs. 2 and 6).

7.9. Eighth eruption (final vulcanian activity)

After the last Plinian phase ceased, the eruptive activity resumed with a change in style from Plinian to vulcanian: the fallout activity was in fact replaced by a widespread pumice-bearing pyroclastic flow (Layer 4), emplaced perhaps as a result of another "boiling-over" mechanism like the 1877 eruption of Cotopaxi volcano (Wolf, 1878; Barberi et al., 1995) or witnessed during the 8–10 May 1997 eruption of the Bezymianny volcano (Kamchatka) (Belousov et al., 2002).

8. Eruption-triggering mechanism and fluctuating eruptive style

The most peculiar characteristic of the C.P. eruptive sequence is the cyclical alternation from vulcanian to Plinian style which occurred in a time lapse of about 500 years and was separated by at least three time breaks (Fig. 13). This variation yielded to the production of "boiling over"-related "cauliflower" scoria flows and bread-crusted bombs (vulcanian phase), alternated with light pumice Plinian fallout deposits. Such a physical volcanic style alternation is corroborated also by a

change in magma composition showing an unexpected trend. Vulcanian style products, in fact, were discovered to be systematically more silicic than explosive Plinian fallout products as shown in the TAS plot of Fig. 5. The chemical and physical alternation of the two eruptive styles could have triggered a modification in local conduit conditions below the magma fragmentation level where a closed-dome summit system (vulcanian eruption of andesitic magma) could have been collapsed and replaced by an open vent eruption (injection of a basaltic andesite magma). It is important to notice that, although pyroclastic flows are commonly associated with the collapse of eruptive columns, for the Citlaltépetl volcano, almost all the scoria-pumice flows (except Layer 4) occurred before the Plinian eruptions, and therefore, they are not associated with the collapse of a Plinian column but to a flow-forming vulcanian style preceding every main pumice fallout event. On the other hand, only at proximal facies, the major fallout layers (A, E+F, H) are intercalated with thin ash-sized horizons and are interpreted as small proximal surge deposits possibly associated with brief eruptive column fluctuations. Such a column fluctuation is a characteristic of the Plinian eruptions of the C.P., where the thrust region may suddenly lack the energy to keep a maintained column and partially collapse, creating radial surge waves at the proximal volcano area. The existence of a Plinian column instability is also suggested by the presence of a vertical variation in clast-size along the main fallout layers (Figs. 2 and 13), as demonstrated also during the deposition of the Plinian Campanian Ignimbrite at the Phlegrean Fields (Rosi et al., 1999) or during the emplacement of the Greenish Pumice at Vesuvius volcano (Cioni et al., 2003). All of the C.P main tephra layers representing high eruptive columns are associated with Plinian eruptions. Perhaps only Layer A may be considered close to the limit between sub-Plinian and Plinian, in accordance with the dispersion index criteria of Walker (1973) which are estimated lower than 500 km^2. However, all the calculated eruptive columns are higher than 20 km and thus can be classified as Plinian.

9. Conclusions

The C.P. sequence consists of a complex succession of pumice fallout deposits alternating with pyroclastic flow deposits. Such a depositional variability indicates that the C.P. changed its eruptive style several times passing from a dome-forming vulcanian style to an extremely explosive Plinian one. This behavior can be compared with the 1984 cyclic eruption of Lascar volcano where every lava dome formation was followed by an explosive eruption due to the increasing of the internal gas pressure caused by the subsidence of the dome inside the conduit (Matthews et al., 1997). The C. P. sequence was explained with the hypothesis of a pyroclastic flow-forming vulcanian style thermally excited by a cyclical injection of hot magma into the magmatic chamber, which increases the internal system energy and triggers the Plinian eruption. As seen in the reconstruction, Such a phenomenon was repeated at least three times during the entire C.P. history. In addition, the composition differences suggest contrasting viscosities between the mafic products and the more evolved magmas which could be the trigger of the two contrasting eruptive styles. The C.P. sequence produced high eruptive columns that easily injected pyroclastic material into the stratosphere causing a global-scaled tephra spreading. Such a tephra distribution and the complex variation in the C.P. eruptive style create difficulties in building a worst case scenario related to a similar possible volcanic crisis. However, we suggest that if the Citlaltépetl volcano should reactivate in the same manner as described in this work, the supposed eruption could form pyroclastic columns as high as 30 km. Due to the dominant wind direction, which varies with the season (November to May towards East; July to September towards West; while October is variable. Cortés-Luna, 1996), the plume could cover with a 5-cm-thick pumice fallout layer at least 1000 km^2 around the cone up to at least a downwind distance of 35 km from the vent. However, more hazardous could be the associated pyroclastic flows and lahars that would channel along the radial valleys of the cone. Affectation areas within a radius of about 35 km may cause a catastrophic scenario, affecting about 350,000 inhabitants (Carrasco-Núñez, 1999).

Acknowledgment

This paper is the result obtained by funding sources: DGEP (SPIAP/PB/2511/2001), scholarship to Andrea Rossotti, CONACyT Grant 44549-F to Gerardo Carrasco-Núñez and Project CONACyT-CNR Number J200/336/04 between the National Autonomous University of Mexico and the University of Pisa, Italy, to Gerardo Carrasco-Núñez and Mauro Rosi. In addition, we acknowledge Carolina Muñoz, Bartolo Rodríguez and Juan Vázquez of the Centro de Geociencias of UNAM, Juriquilla for their help during the laboratory analysis and Dr. Patrizia Landi, Dr. Laura Pioli and Dr. Simone Arrighi of Pisa University for their precious contribution and help during the fieldwork stage.

Patricia Girón and Rufino Lozano performed the chemical analysis using XRF techniques at UNAM. We thank also Dr. Guido Giordano of Universita' di Roma 3, Dr. Sharon Allen of University of Tasmania, Dr. Carlos Mendoza of UNAM and Susan Spizzirri for their respective detailed and helpful reviews.

References

Adams, N.K., Shanaka, L., De Silva, S., Self, S., Salas, G., Schubring, S., Permenter, J.L., Arbesman, K., 2001. The physical volcanology of the 1600 eruption of Huaynaputina, southern Peru. Bull. Volcanol. 62, 493–518.

Barberi, F., Cioni, R., Rosi, M., Santacroce, R., Sbrana, A., Vecci, R., 1989. Magmatic and phreatomagmatic phases in explosive eruptions of Vesuvius as deduced by grain-size and component analysis of the pyroclastic deposits. J. Volcanol. Geotherm. Res. 38, 287–307.

Barberi, F., Martini, M., Rosi, M., 1990. Nevado de Ruiz Volcano (Colombia): pre-eruption observations and the November 13, 1985 catastrophic event. J. Volcanol. Geotherm. Res. 42, 1–12.

Barberi, F., Coltelli, M., Frullani, A., Rosi, M., Almeida, E., 1995. Chronology and dispersal characteristics of recently (last 5000 years) erupted tephra of Cotopaxi volcano (Equador): implications for a long-term eruptive forecasting. J. Volcanol. Geotherm. Res. 69, 217–239.

Belousov, A., Voight, B., Belousova, M., Petukhin, A., 2002. Pyroclastic surges and flows from the 8–10 may 1997 explosive eruption of Bezymianny volcano, Kamchatka, Russia. Bull. Volcanol. 64, 455–471.

Bonadonna, C., Houghton, B.F., 2005. Total grain-size distribution and volume of tephra-fall deposits. Bull. Volcanol. 67 (5), 441–456.

Bonadonna, C., Ernest, G.G., Sparks, R.S.G., 1998. Thickness variation and volumes estimates of tephra fall deposit; the importance of particle Reynolds number. J. Volcanol. Geotherm. Res. 81, 173–187.

Bursik, M., 1993. Subplinian eruption mechanism inferred from volatile and clast dispersal data. J. Volcanol. Geotherm. Res. 57, 57–70.

Capra, L., Macias, J.L., Espindola, J.M., Siebe, C., 1997. Holocene Plinian eruption of La Virgen volcano, Baja California, México. J. Volcanol. Geotherm. Res. 80, 239–266.

Carey, S., Sigurdsson, H., 1986. The 1982 eruption of El Chichon volcano, Mexico (2): Observations and numerical modeling of tephra-fall distribution. Bull. Volcanol. 48, 127–141.

Carey, S., Sigurdsson, H., 1987. Temporal variations in column height and magma discharge rate during the 79 A.D. eruption of Vesuvius. Geol. Soc. Amer. Bull. 99, 303–314.

Carey, S., Sigurdsson, H., 1989. The intensity of Plinian eruptions. Bull. Volcanol. 51, 28–40.

Carey, S., Sparks, R.S.J., 1986. Quantitative models of the fallout and dispersal of tephra from volcanic eruption columns. Bull. Volcanol. 48, 109–125.

Carey, S.N., Gardner, J.E., Sigurdsson, H., 1995. The intensity and magnitude of Holocene Plinian eruptions from Mount St. Helens volcano. J. Volcanol. Geotherm. Res. 66, 185–202.

Carrasco-Núñez, G., 1993. Structure, eruptive history and some major hazardous events of Citlaltépetl volcano (Pico de Orizaba), Mexico. Ph.D. dissertation, Michigan Technological University, USA, 182 pp.

Carrasco-Núñez, G., 1997. Lava flow growth inferred from morphometric parameters: a case study of Citlaltépetl volcano, Mexico. Geol. Mag. 134 (2), 151–162.

Carrasco-Núñez, G., 1999. Holocene block-and-ash flows from summit dome activity of Citlaltépetl volcano, Eastern Mexico. J. Volcanol. Geotherm. Res. 88, 47–66.

Carrasco-Núñez, G., 2000. Structure and proximal stratigraphy of Citlaltépetl volcano (Pico de Orizaba), México. Spec. Pap. - Geol. Soc. Am. Bull. 334, 247–262.

Carrasco-Núñez, G., Ban, M., 1994. Geologic Map and Structure Sections of the Summit Area of Citlaltépetl Volcano, Mexico. Serie de cartas geológicas y mineras, vol. 9. Instituto de Geología UNAM, México.

Carrasco-Núñez, G., Rose, W.I., 1995. Eruption of a major Holocene pyroclastic 786 clastic flow at Citlaltépetl volcano (Pico de Orizaba), Mexico, 8.5–9.0 Ka. J. Volcanol. Geotherm. Res. 69, 197–215.

Carrasco-Núñez, G., Vallance, J.W., Rose, W.I., 1993. A voluminous avalanche-induced lahar from Citlaltépetl volcano, Mexico: Implications for hazard assessment. J. Volcanol. Geotherm. Res. 59, 35–46.

Carrasco-Núñez, G., Gomez-Tuena, A., Lozano, L., 1997. Geologic map of Cerro Grande volcano and surrounding area, Central Mexico. Geol. Soc. America Maps and Chart series. MCH, vol. 081, p. 10.

Cashman, K.V., Hoblitt, R.P., 2004. Magmatic precursors to the 18 may 1980 eruption of Mount St. Helens, USA. Geology 32 (2), 141–144.

Cioni, R., Marianelli, P., Santacroce, R., Sbrana, A., 2000. Plinian and subplinian eruptions. Encyclopedia of Volcanoes. Academic Press, pp. 477–494.

Cioni, R., Sulpizio, R., Garruccio, N., 2003. Variability of the eruption dynamics during a subplinian event: the Greenish Pumice eruption of Somma–Vesuvius (Italy). J. Volcanol. Geotherm. Res. 124, 89–114.

Cortés-Luna, J.R., 1996. Comportamiento del viento en la atmósfera superior de la parte central de México y su aplicación en vulcanología. Tesis de Licenciatura UNAM, 146 pp.

Di Muro, A., Neri, A., Rosi, M., 2004. Contemporaneous convective and collapsing eruptive dynamics: the transitional regime of explosive eruptions. Geophys. Res. Lett. 31, 1–4.

Fierstein, J., Nathenson, M., 1992. Another look at the calculation of fallout tephra volumes. Bull. Volcanol. 54, 156–167.

Formenti, Y., Druitt, T.H., Kelfoun, K., 2003. Characterization of the 810 1997 vulcanian explosions of Soufriere Hills volcano, Monserrat, by video analysis. Bull. Volcanol. 65, 587–605.

Höskuldsson, A., Robin, C., 1993. Late Pleistocene to Holocene eruptive activity of Pico de Orizaba, Eastern Mexico. Bull. Volcanol. 55, 571–587.

Houghton, B.F., Wilson, C.J.N., 1989. A vesicularity index for pyroclastic deposits. Bull. Volcanol. 51, 451–462.

Matthews, S.J., Gardeweg, M.C., Sparks, R.J.S., 1997. The 1984 to 1996 cyclic activity of Lascar volcano, northern Chile; cycles of dome growth, dome subsidence, degassing, and explosive eruptions. Bull. Volcanol. 59 (1), 72–82.

Mercalli, G., 1906. La grande eruzione vesuviana iniziata il 4 aprile 1906. Memoria Pontificia Accademia Romana Nazionale dei Lincei, vol. XXIV, pp. 307–338.

Newhall, C.G., Self, S., 1982. The Volcanic Explosivity Index (VEI): an estimate of the explosive magnitude for historical volcanism. J. Geophys. Res. 87 (C), 1231–12328.

Pyle, D.M., 1989. The thickness, volume and grainsize of tephra fall deposits. Bull. Volcanol. 51, 1–15.

Pyle, D.M., 1995. Assessment of the minimum volume of tephra fall deposits. J. Volcanol. Geotherm. Res. 69, 379–382.

Robin, C., Cantagrel, J.M., 1982. Le Pico de Orizaba (Mexique): Structure et evolution d'un grand volcan andesitique complexe. Bull. Volcanol. 45 (4), 299–315.

Rodríguez, S.R., Siebe, C., Komorowski, J.C., Abrams, M., 2002. The Quetzalapa Pumice: A voluminous late Pleistocene rhyolite deposit in eastern Trans-Mexican Volcanic Belt. J. Volcanol. Geotherm. Res. 113, 177–212.

Rosi, M., Vezzoli, L., Castelmenzano, A., Grieco, G., 1999. Plinian pumice fall deposit of the Campanian Ignimbrite eruption (Phlegrean Fields, Italy). J. Volcanol. Geotherm. Res. 91, 179–198.

Rossotti, A., Carrasco-Núñez, G., 2004. Stratigraphy of the 8.5–9.0 Kyr. B.P. Citlaltépetl Pumice fallout sequence. Rev. Mex. Cienc. Geol. 21 (3), 353–370.

Scandone, R., Malone, S.D., 1985. Magma Supply, Magma discharge and readjustment of the feeding system of Mt. St. Helens during 1980. J. Volcanol. Geotherm. Res. 23, 239–262.

Sigurdsson, H., Carey, S., 1989. Plinian and co-ignimbrite tephra fall from the 1815 eruption of Tambora volcano. Bull. Volcanol. 51, 243–270.

Sigurdsson, H., Carey, S., Cornell, W., Pescatore, T., 1985. The eruption of Vesuvius in AD 79. Natl. Geogr. Res. 1, 332–387.

Sparks, R.S.J., 1986. The dimensions and dynamics of volcanic eruption columns. Bull. Volcanol. 48, 3–14.

Walker, G.P.L., 1973. Explosive volcanic eruptions—A new classification scheme. Geol. Rundsch. 62, 431–446.

Walker, G.P.L., 1980. The Taupo Pumice: product of the most powerful known (ultraplinian) eruption? J. Volcanol. Geotherm. Res. 8, 69–94.

Walker, G.P.L., 1981. Plinian eruptions and their products. Bull. Volcanol. 44 (2), 223–240.

Walker, G.P.L., Croasdale, R., 1970. Two Plinian-type eruptions in the Azores. J. Geol. Soc. (Lond.) 127, 17–55.

Wilson, C.J.N., Hildreth, W., 1997. The Bishop Tuff: new insights from eruptive stratigraphy. J. Geol. 105, 407–439.

Wilson, L., Walker, G.P.L., 1987. Explosive volcanic eruptions IV. Ejecta dispersal in Plinian eruptions: the control of eruption conditions and atmospheric properties. Geophys. J. R. Astron. Soc. 89, 657–679.

Wilson, L., Sparks, R.S.J., Huang, T.C., Watkins, N.D., 1978. The control of eruption column heights by eruption energetic and dynamics. J. Geophys. Res. 83, 1829–1836.

Wohletz, K.H., 1983. Mechanism of hydrovolcanic pyroclast formation: grain-size, scanning electron microscopy, and experimental studies. J. Volcanol. Geotherm. Res. 17, 31–63.

Wolf, T., 1878. Memoria sobre el Cotopaxi y su ultima erupción acaecida el 26 de Junio de 1877. Imprenta del comercio, p. 63.